RSP-0298

McMaster University ENGINEERING	**FINAL REPORT**	
Project:	***R522.1a: International CFD Benchmark Problem***	
	Contract 87055-11-0519	
Title:	***Final Report***	
Date:	NOVEMBER 30, 2012 (REVISION 1)	
Prepared by	Dr. Alex Rashkovan Visiting Scientist McMaster University	Prof. D.R. Novog Associate Professor McMaster University
Reviewed by	Prof. D.R. Novog Associate Professor McMaster University	

Contents

1 BACKGROUND

Computational Fluid Dynamics (CFD) is being increasingly utilized in the design, analysis and licensing of nuclear power stations. Internationally CFD has been used to assess mixing vane spacer designs, to examine boron dilution problems, t-junction induced aging and other localized or 3-dimensional phenomena. In Canada, CFD has been applied in header geometries to study header pressure and temperature gradients, flow and turbulence generation inside fuel bundles and in safety and licensing applications related to moderator flow and temperature distributions. This report documents the scope and results for a CFD study and comparison to experimental results from the latest OECD-NEA computational fluid dynamics benchmark.

Prediction of subchannel flows, even in isothermal conditions, is very challenging. Complicated flow structures, mixing in the gap region, and even unsteady pulsing type behavior all produce uncertainties in any predictive models. This is made more complicated by the presence of grid spacers in LWR assemblies, or endplates in CANDU fuel, which cause rigorous mixing as well as greatly increasing the local turbulence levels. In many historical studies, subchannel thermalhydraulic codes such as COBRA or ASSERT-PV have been used to predict subchannel flows within fuel bundles. However these subchannel codes rely on empirically derived mixing coefficients, hydraulic loss factors, and empirical shear stress relationships in closing the system of equations. The advantage of a CFD code for subchannel predictions is that it does not rely so heavily on geometrically dependent mixing factors and empiricisms. Hence CFD results have the potential for wider applicability, notwithstanding their needs for adequate validation and testing. The study of CFD code applicability and accuracy has been the topic of a large number of validation exercises as well as international benchmarks.

The OECD-NEA has organized a new benchmark to study CFD applications to bundle flows and turbulence levels. This benchmark involved taking new experimental data in a rod-bundle geometry including grid spacers and taking detailed point-wise time-average and rms velocity measurements. These data were hidden from the benchmark participants until after the deadline for submitting contributions. Thus the CFD predictions were “blind” from this respect. The benchmark team released the specifications, geometries and boundary conditions for this experiment[1] in 2011, and participants in the CFD benchmark were asked to submit their results in May 2012. After submissions, the OECD performed an assessment of the submitted CFD results against the experimental data and also released the results to the CFD participants so they could do their own comparisons.

1 All of the details, CAD drawings and specification are available from the NEA organizing committee and are not repeated in this report. This work conforms to those specifications to the greatest extent practicable and documents the deviations where required.

2 OBJECTIVE

The overall objective of this work was to produce a submission for the OECD-NEA MATiS Computational Fluid Dynamics benchmark from McMaster University using the commercial CFD package STAR-CCM+. To accomplish this objective we conducted several separate-effect studies to ascertain the most appropriate mesh structure, geometrical modelling details, turbulence models and boundary conditions. Once these were established we developed a reference benchmark geometry and performed several mesh and turbulence sensitivity studies. These were used to finalize our submission package. The objectives of this project were completed on schedule.

3 SCOPE

The scope of work was to produce CFD models and results for the OECD-NEA bundle benchmark using the STAR-CCM+ suite of programs and to submit these results for inclusion in the blind benchmark.

At the outset of this project the McMaster team adopted a strategy where we wished to develop a CFD model for the benchmark which would be comparable to those which would be needed in realistic studies of bundle flows which include i) heat transfer and fluid property changes ii) long assembly lengths. As such, we did not wish to adopt mesh or turbulence modelling strategies for the benchmark which would not be practical for more realistic applications. Thus the focus of our work was on selecting mesh and 2-equation turbulence models that could produce results within a few tens of hours. While more accurate meshing and turbulence models may be available in STAR-CCM+, these were used to assess the capabilities of the models at each stage. We performed a series of progressively more complex simulations using simplified geometries in order to determine the best possible mesh and turbulence options which would be needed in subsequent simulations of the entire benchmark geometry.

The major scope items included:

- Generation, documentation and qualification of a reference grid for the benchmark for the non-swirl grid spacers. This includes generation of a preliminary grid and solution, analysis of these preliminary results, and setting up a reference based on the preliminary results and scoping study.
- Generation of a subchannel input dataset of the benchmark experiment and performing a set of subchannel predictions of the flows and pressure drop from the non-swirl grid spacers[2].
- CFD simulations using the reference grid as well as convergence and sensitivity studies for these simulations. This also includes comparison to the subchannel results.
- Grid refinement studies.

[2] This scope item was removed with the consent of the CNSC Technical Authority.

- Development of a comparable grid for the swirling spacer geometry and simulations of this configuration in STAR-CCM+.
- Post-processing and preparation of the package for OECD-NEA benchmark submission.
- Participation in the final OECD closure meeting in September 2012.
- Generation of all progress reports and other communications with the CNSC contacts as well as minimum of 2 face-to-face meetings during the project.
- Preparation of the draft final report, incorporation of CNSC comments and issue of the final report (with presentation to the CNSC) and including a CD ROM with all relevant information.

This report constitutes the final report for this project. All other deliverables were completed as planned.

4 LITERATURE REVIEW

Flow and heat transfer through vaned-spacer grids has been studied both experimentally [e.g., 1,2, 3, 4, 5, 6, 7] and numerically [e.g., 8, 9, 10] in the past. Especially interesting are the results of PIV studies using the refractive index matched rod bundle thus allowing detailed velocity measurements in the regions close to the walls [11]. Although most cases reported are proprietary and the exact geometry and flow conditions are not readily available, some of the results presented were found to be useful in the task of modelling the MATIS-H benchmark.

In descending order of complexity, turbulent flow modelling strategy goes from direct numerical simulation (DNS) through large eddy simulation (LES) towards unsteady and steady Reynolds averaged Navier-Stokes equations (RANS). DNS is an approach that solves numerically the equations of motion without modelling. This would have been the method of choice, but it has long been realized that DNS is not feasible for high Reynolds number turbulent flows because of the extremely large computational resources (fine mesh, small time step and high-order discretization scheme) required to capture turbulent motions to the smallest dynamically important scale (Kolmogorov microscale). All other methods are based on the modelling of some or all turbulent motions. A widely used CFD method for industrial flows is the solution of the Reynolds-Averaged Navier Stokes (RANS) equations, coupled with modelled equations for turbulence. This method has the lowest requirements in terms of computational resources, but its accuracy depends on the geometry and flow conditions, as well as the turbulence model capabilities. Moreover, RANS methods cannot resolve time-dependent motions. Unsteady RANS (URANS) methods maintain the turbulence modelling used in RANS, but can also resolve time-dependent large-scale motions, if such are present in the flow. URANS require significantly larger computational resources than RANS and would produce the same solutions as RANS in flows in which unsteady effects are not significant. Large Eddy Simulations (LES) solve low-pass filtered dynamic equations, so that motions with a scale smaller than a specified value (sub-grid-scale motions - SGS) are not resolved but taken into consideration in the solution with the use of an SGS model. The filter cut-off scale must be within the inertial spectral subrange, which can be quite small in high Reynolds number turbulent flows, especially near walls. Thus, mesh size and time step must be sufficiently small for LES to work. Coarse LES would miss a significant part of the turbulence activity and could also suffer from other

unpredictable inaccuracies due to the inapplicability of the SGS model. A host of hybrid methods, combining LES and URANS or otherwise simplifying LES solutions in at least some parts of the computational domain have been introduced in an effort to maintain the accuracy of LES at a lower computational cost.

CFD applications continue to increase in the nuclear safety field. In the LWR and HWR communities there are a variety of safety issues where application of CFD is expected to provide insight and assist in closing the issues. These issues are summarized in the following table.

	NRS problem	System classification	Incident classification	Single- or multi-phase
1	Erosion, corrosion and deposition	Core, primary and secondary circuits	Operational	Single/Multi
2	Core instability in BWRs	Core	Operational	Multi
3	Transition boiling in BWR/determination of MCPR	Core	Operational	Multi
4	Recriticality in BWRs	Core	BDBA	Multi
5	Reflooding	Core	DBA	Multi
6	Lower plenum debris coolability/melt distribution	Core	BDBA	Multi
7	Boron dilution	Primary circuit	DBA	Single
8	Mixing: stratification/hot-leg heterogeneities	Primary circuit	Operational	Single/Multi
9	Heterogeneous flow distribution (e.g. in SG inlet plenum causing vibrations, HDR expts., etc.)	Primary circuit	Operational	Single
10	BWR/ABWR lower plenum flow	Primary circuit	Operational	Single/Multi
11	Waterhammer condensation	Primary circuit	Operational	Multi
12	PTS (pressurised thermal shock)	Primary circuit	DBA	Single/Multi
13	Pipe break – in-vessel mechanical load	Primary circuit	DBA	Multi
14	Induced break	Primary circuit	DBA	Single
15	Thermal fatigue (e.g. T-junction)	Primary circuit	Operational	Single
16	Hydrogen distribution	Containment	BDBA	Single/Multi
17	Chemical reactions/combustion/detonation	Containment	BDBA	Single/Multi
18	Aerosol deposition/atmospheric transport (source term)	Containment	BDBA	Multi
19	Direct-contact condensation	Containment/ Primary circuit	DBA	Multi
20	Bubble dynamics in suppression pools	Containment	DBA	Multi
21	Behaviour of gas/liquid surfaces	Containment/ Primary circuit	Operational	Multi
22	Special considerations for advanced (including Gas-Cooled) reactors	Containment/ Primary circuit	DBA/BDBA	Single/Multi

Table 1: Application of CFD in Nuclear Reactor Safety[12]

It has to be noted that using even LES for the full rod bundle geometry with heat transfer would be an almost prohibitively costly task. Due to the much lower computational cost needed, most of the numerical studies reported on flow through full sized rod bundle with vaned spacer grids were steady RANS simulations using various two-equation and RSM models. While Holloway *et al* [9] used Fluent and found SST-kω with all-*y+* wall treatment resulted in the closest match with experiment compared with the RSM and RKE models; Conner *et al* [8] used STAR-CCM+ and found RNG k-ε model with high-*y+* grid was better than its counterparts. In [10] the standard k-ε model was incorporated in CFX and reported good agreement with experimental results on flow through a spacer grid with split vanes. No single model is suggested in the literature to perform better in the case of the flow through spacer grids with mixing vanes. Hence, separate effect studies have been performed for the MATIS-H benchmark experiment in order to provide additional information on turbulence specification for our submission.

As a result of the literature review we identified promising test cases wherein we could assess the features and options in STAR-CCM+ against real bundle data. The objective of this was to obtain a series of recommended options and topology which would allow the best solution in the subsequent stages of the project. The results are documented in the following sections.

5 METHODOLOGY

5.1 Tools

This work utilizes the commercial STAR-CCM+ software package which has been developed by CD-ADAPCO as a modern computational fluid dynamics tool and has many unique and promising features (e.g., direct connection to the RELAP safety analysis code). Its unique features include:

- Integrated CAD & CAE modeling.
- Novel meshing technology - With both manual and automatic surface preparation tools, and surface wrapping, as well as state of the art polyhedral and trimmed cell meshing including polyhedral, fully conformal meshes can automatically be created. Prism layers are robustly generated to ensure accurate capture of boundary layers. The latest tools for mesh refinement and parallel processing of mesh generation to allow for increased numbers of sensitivity studies. All mesh operations and activities are recorded so meshes are of high quality and can be easily verified.
- Parallel and adaptable solver features with over 64 computational nodes available at McMaster.
- Advanced wall features and turbulence modeling options.
- Dynamic data - The simulation may be monitored at every stage of the solution evolution with results dynamically updated. As the simulation runs and the solution develops, data may be continuously interrogated and solver settings changed on the fly. Effective analysis and communication.
- STAR-CCM+ has an extensive range of visual analysis tools to help deliver insight from the results.

- A suite of turbulence models comparable to those of other commercial CFD codes and easily accessible (standard RANS models, LES, DES).

5.2 Separate-Effect Studies

As stated previously the goal of this work is to demonstrate accurate simulation results using a number of mesh points and turbulence models such that it would represent a reasonable compromise between the fidelity of the purely hydraulics CFD and the potential to incorporate realistic heat transfer and fluid property variations. As such we excluded turbulence models (such as DNS or LES) and extremely fine nodalizations from the models examined. While such models represent the state-of-the art for isothermal CFD flows, their use in the complex geometries inside the entire length of the reactor core and including the effects of non-uniform heat transfer and fluid property variations is limited. Even so, there still existed a wide variety of geometry and meshing treatments available for study, and hence we commissioned a series of numerical separate-effect experiments to determine the best possible combination of modelling parameters. These separate-effect studies involved:

i. Positioning Button Effects Study – This study examined flow through a small number of representative subchannels where the effect of the localizing buttons on the flow was investigated. Since these positioning devices hold the rods firmly in place within the grid spacer there are 2 buttons located in every gap between the rods, in the space between the outer rods and the sides of the grip plates. Several steady and unsteady (URANS) simulations were performed examining the effects of a single button as well as multiple buttons on the flow field and turbulence levels.

ii. Sensitivity of Vane Tip Effects on Downstream Flow – In this study we examined several turbulence models and meshes on the flow and turbulence levels immediately downstream of the mixing vanes. The goal of these studies was to examine the sensitivity of predictions of the vane effects to models and mesh selection.

5.3 Simulations for Existing Rod Bundle Literature

KAERI reported the results of very detailed flow and turbulence measurements for flow in a 5 x 5 rod bundle array with similar dimensions as the OECD MATiS benchmark [1,2], hence these experiments were used to further test and refine our modelling approach.

iii. Comparisons to Previous KAERI Results – In this study we examined several possible mesh strategies for the entire domain by examining predictions for a similar experiment in literature. These previous experiments utilized grid spacers and mixing vanes and hence we performed CFD simulations for this previous geometry

iv. Entrance Boundary Conditions Study – A study was performed to determine the most appropriate inlet boundary condition for the benchmarks case and was compared to the limited measurements provided in the benchmark specifications.

v. Effect of Cutout Geometries – since the available literature on rod arrays did not fully specify the vane geometry, we conducted several studies to ascertain the sensitivity of our results to the cutout assumptions.

vi. Effect of Symmetry Assumptions – While there exists some lateral and rotational symmetries in the OECD benchmark bundles that could be exploited to reduce the computational domain, we

felt that utilizing these reductions would not be possible in a realistic bundle with non-symmetric heat transfer. Hence from the outset we were of the opinion that the whole geometry should be simulated in such a way that simulation times were more representative of those needed in engineering applications. Furthermore, employing symmetry in potentially unsteady flow fields can suppress the instabilities and hence lead to non-physical or inaccurate solutions. Nevertheless we studied the effect of employing symmetry on the flow field as an additional separate effect study.

5.4 Final Benchmark Submission Simulations

Given the lessons learned from the studies conducted during the separate-effect phase of this work we selected the most appropriate 2-equation model and meshing technique possible. We then generated the reference cases for the swirl and split vane cases. For both of these geometries we generated additional cases with varying mesh densities in order to examine the sensitivity of our final predictions to grid size. Based on the sensitivity of these results, as well as considering the overall objective of producing a meaningful solution within a reasonably relevant computational time, we selected our cases for submission. Details of the cases and results can be found in the following sections.

6 SEPERATE EFFECT AND INTEGRATED STUDIES

6.1 Separate Effect Studies

6.1.1 Effect of Positioning Buttons on the Flow

Flow around a single centralizing button was simulated as shown in Figure 1. The effect of these buttons on the flow field was selected for study since it essentially represents a cylinder in cross-flow within a confined region. Since cylinders in cross flow are known to introduce vortices we focused our initial studies on the potential unsteady behaviour of the flow near these buttons.

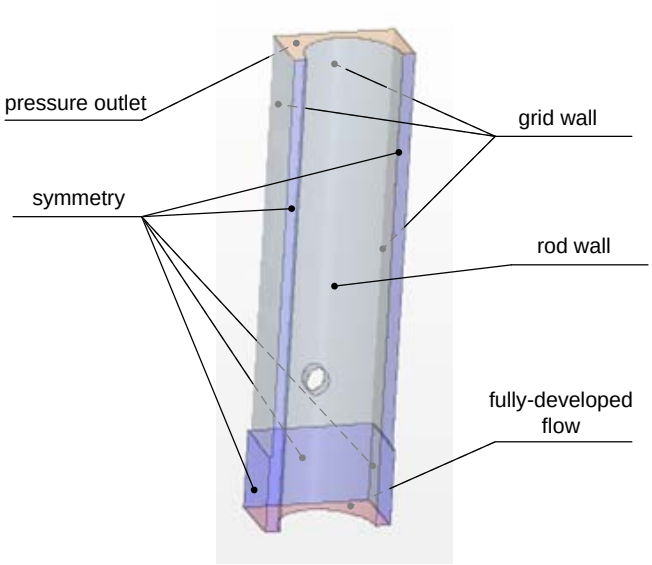

Figure 1. Geometry for studying flow over the centralizing buttons.

The geometry in Figure 1 was meshed and simulated in STAR-CCM+ with a wide range of mesh structures, varying turbulence models, and some unsteady methods. Numerical instabilities in steady simulations (see Figure 2 left) were encountered and as was revealed in the unsteady simulations the flow around a single button did exhibit some transient behaviour. The instabilities were of the similar nature as those appearing in flow over a cylinder with vortex shedding effect. Although the geometry of the buttons is that of the cylinder confined between the convex and the flat walls of the rod and the grid respectively, the resulting frequency of vortex shedding predicted in the unsteady simulations turned out to be of the same order as that expected in the classical situation, 80 instead of 60Hz, using SST-kω model.

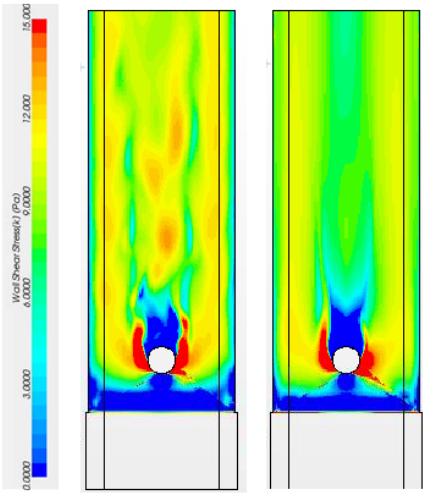

Figure 2. Wall shear stress in steady simulations. SST-kω – left, RKE – right[3].

While resolving the flow instability could eventually result in more accurate flow field, we spent a considerable amount of deliberation as to the merit of their inclusion since including the effects of all buttons would necessitate a very fine structure within the grid plates (where no measurements were made) and could then ultimately require an unsteady final solution. Such mesh and unsteady simulations would increase our computational time by orders of magnitude and would essentially mean that any further heat transfer type simulations would not be engineering practicable.

To provide more information in the decision making process we computed the flow field around 2 inline centralizing buttons to observe the unsteady effects of interacting cylinders, and then we added some simple vane tips to the geometries outlined in Figure 2. We observed the results immediately downstream of the vane tips to be steadier than the flow around a single button implying that there was some destructive interference of the unsteady velocity features which caused more steady behaviour

[3] Note: It has to be mentioned that the steady flow solution for the RKE model appears converged and moving to transient simulation does not cause any significant instabilities. On the other hand, while steady solution of the SST-kω model appears to be unstable and not converged, its transient counterpart shows solid basis for the vortex shedding phenomena for a number of time steps and meshes checked, giving the same, i.e. verified shedding frequency. Figure 2 presents the spacer grid wall shear stress for the steady calculations.

downstream of the grid. Hence it was desirable to use coarse meshes around the button areas in order to dampen the local instabilities with the benefit of improving simulation times. However, such simplification means that the additional turbulence generated by the interaction of local flow field around each button may be lost, and hence our downstream turbulence levels may be under predicted. Further details of the studies focused on the button and vane interactions are provided in the following section.

6.1.2 Effect of Vane Tips and Modelling Methods

The model selected for simulating flow around the vanes is that of the laterally-infinite bundle with symmetry lateral conditions as shown in Figure 3.

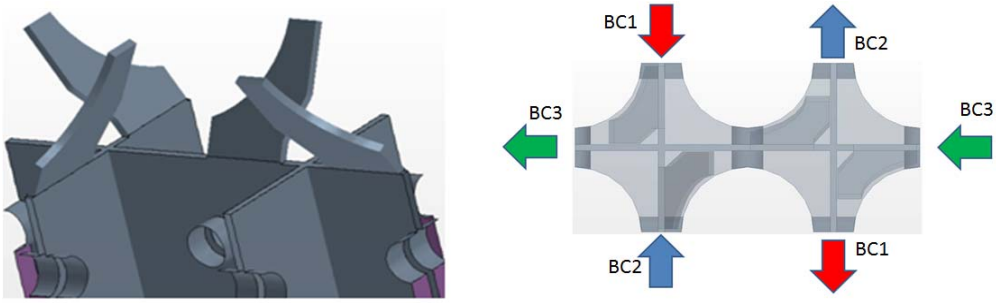

Figure 3. Infinite sub-bundle geometry.

Symmetry boundary conditions were employed on the 3-outter surfaces in order to reduce the size of the computational domain such that a large number of steady and unsteady runs could be performed. Although no finite assembly wall effects can be incorporated in the geometry presented in figure 3 (i.e., the side wall effects in the actual bundle are not included), the domain is quite small and still represents the main features of the flow over the vaned grids. The selection of this sub-domain for studying the fine features of the flow allowed us to examine a very large number of mesh topologies, a large number of turbulence models and solution parameters and quickly observe the effects on the solution. The geometry of the vanes is as close as it could be to the published KAERI experiment data [6, 7], since some local velocity and turbulence measurements were available in the open literature for this design[4].

Steady realizable k-ε (RKE) simulations of the infinite sub-bundle revealed that the solution in the vicinity of the vane tips is unstable with fine mesh (base size 0.4mm, BL 1st row 0.092mm, growth rate 1.728 with 4 rows, surface mesh size 0.3mm). Qualitatively, simulation with the coarse mesh (base size 1mm, BL 1st row 0.47mm, growth rate 1.0 with 3 rows, surface mesh size 1mm) using RKE showed much more stable and converged solution, though slight instabilities were also observed in the convergence data. Details are presented in the following discussion.

[4] No information concerning the way the rods were centralized in the mentioned KAERI work is provided in the papers. Buttons were assumed to be used as in the case of the benchmark setup. Furthermore, the exact geometry of the vanes and especially the cut-outs is also not given in the paper.

Figure 4 presents the wall shear stress on the grid wall for the two meshes described. Figure 5 demonstrates the solution instability in terms of the minimum lateral velocity on a line segment one hydraulic diameter downstream of the mixing vanes (i.e., it examines the change in minimum lateral velocity as a function of iteration number over a region of the predicted flows). It is observed that the fine mesh solution fluctuates, while the coarse grid shows much less instability as a function of iteration (implying that the coarse meshes can be used to filter some of the unsteady behaviour). Table 1 summarizes the stability issues in the steady simulations performed with the fine mesh. Here we adopt the common technique of examining the convergence characteristics of steady simulations in an attempt to examine the presence and features of possible unsteady flow. Subsequent simulations using unsteady CFD treatment are then focused on cases where we observe quasi-non-steady behaviour in the steady solution convergence characteristics.

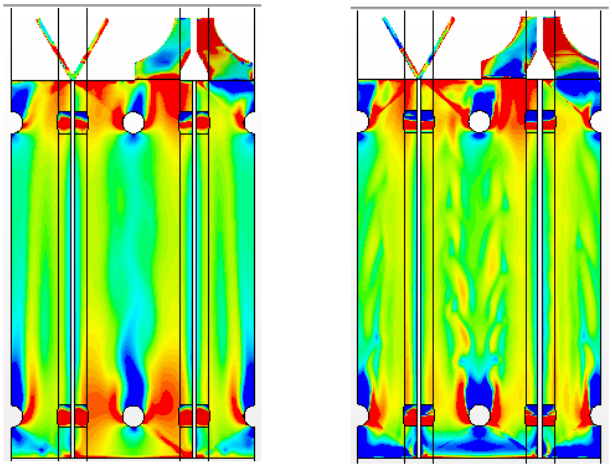

Figure 4. Streamwise wall shear stress. Steady RKE with coarse (left) and fine (right) meshes.

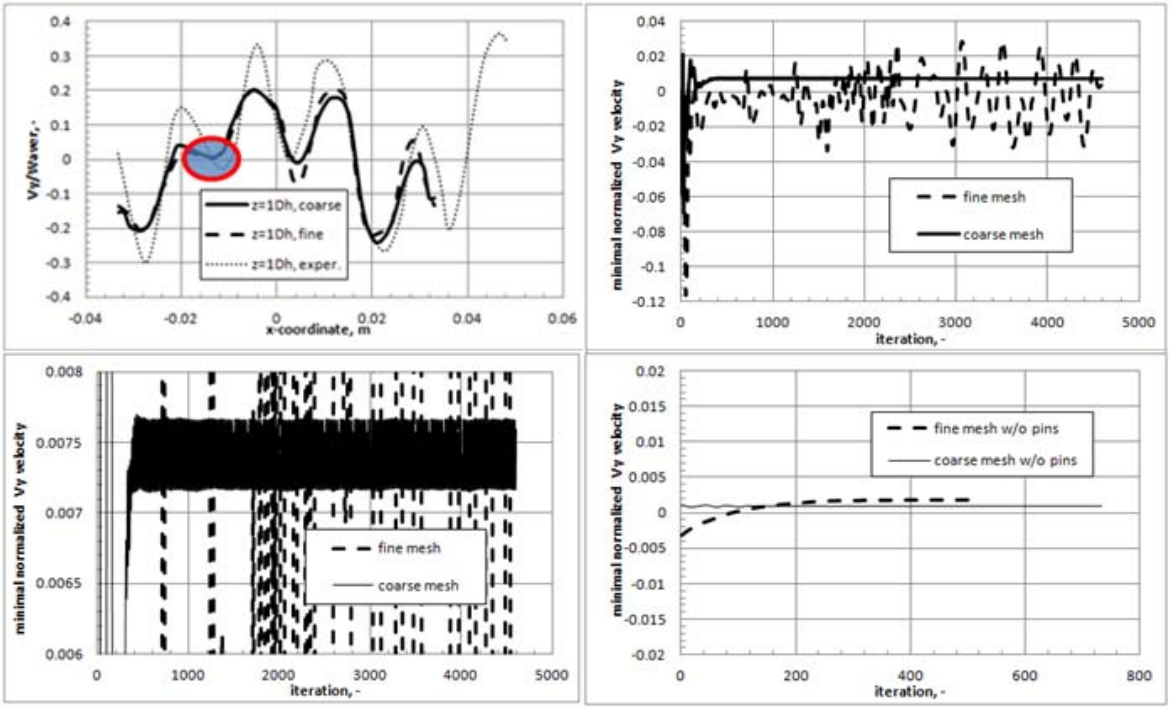

Figure 5. Solution convergence. Top left shows the line segment whose minimal velocity is presented on the rest of the plots in the figure. Top right – minimal velocity convergence as a function of iterations. Bottom left – ordinate axis magnification of the top right plot. Bottom right shows converged solution for the "no-buttons" infinite bundle geometry.

Table 2 shows the matrix of test conducted in examining the impact of the positioning buttons on the steadiness of the flow field downstream of the vane tips as well as the observations of the convergence characteristics. The terms fluctuating and converged indicate the observations of the convergence behaviour in the steady-state simulations. We can see that for the infinite sub-bundle studied here, there are no fluctuating components when the positioning buttons are not present; whereas we observe these fluctuations in most other cases as shown Table 2.

Table 2. Solution convergence for the fine grid, steady state simulations for different geometries.

	RKE	SST-kω
One button (figure 1)	Converged	Fluctuating
Infinite bundle (figure 3)	Minor fluctuations	Major fluctuation
Infinite bundle w/o buttons	Converged	Converged

Grid sensitivity studies were first performed with the infinite bundle geometry for steady simulations using three meshes with the base sizes of 1, 0.5 and 0.25 mm. Boundary layer was meshed in the same manner for all the three core mesh sizes. This was done in order to limit the study to the influence of the core mesh size. The boundary layer was meshed in such a manner so the *y+* values will be of the order of 1.

Figure 6 presents the average streamwise and spanwise velocity profiles at z=1Dh from the vanes tips. It can be concluded that for both graphs no further information is gained for the mesh of 0.25mm.

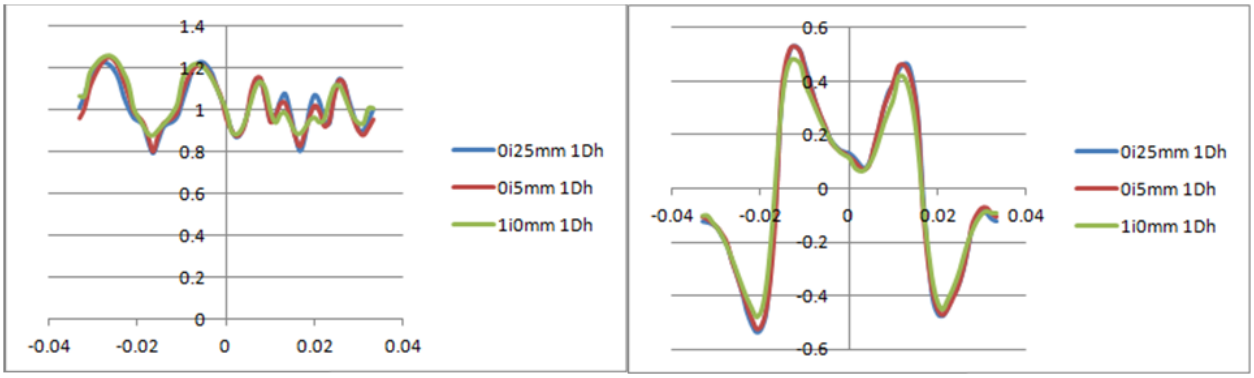

Figure 6. Streamwise (left) and spanwise (right) average velocities for the infinite bundle.

Figure 7 presents the turbulent kinetic energy decay with the downstream distance from the vanes tips. It is seen that here, as in the case of the average velocities, core mesh size of 0.5mm is enough to resolve the flow features.

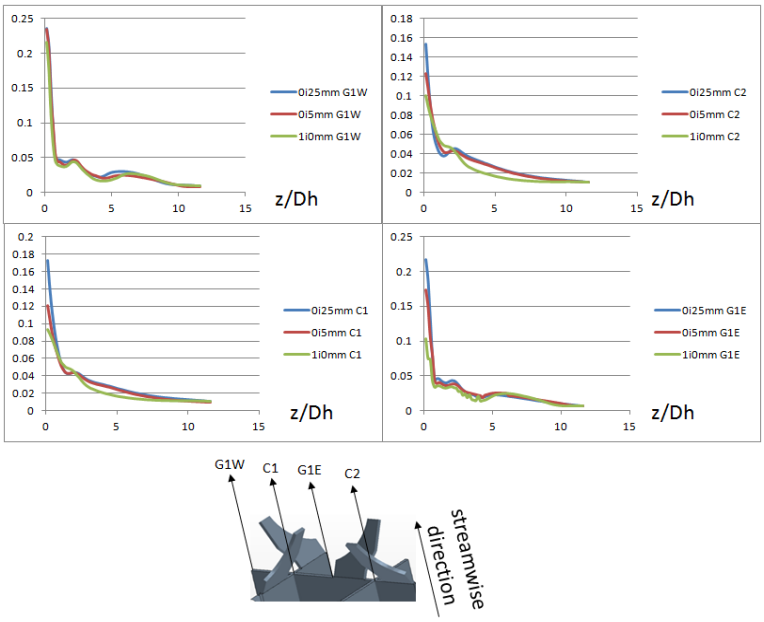

Figure 7. Turbulent kinetic energy. Mesh sensitivity for the infinite bundle.

Figure 8 presents the streamwise vorticity contours along with the mesh in the plane distanced one hydraulic diameter from the vanes tips.

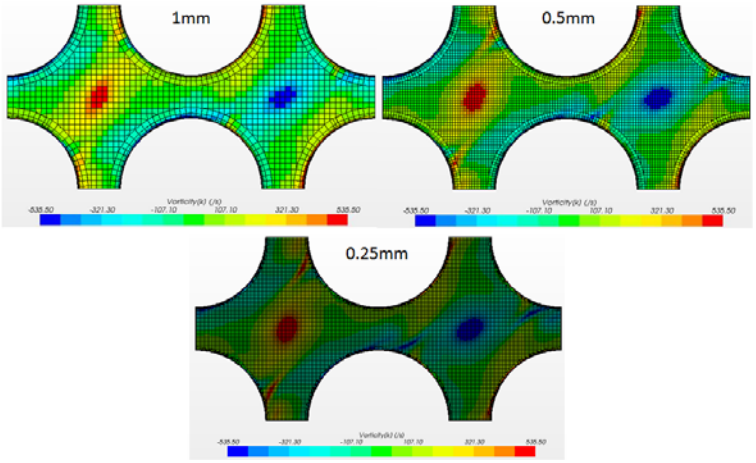

Figure 8. Vorticity contours. Mesh sensitivity for the infinite bundle.

The overall conclusion for the results presented in Figures 6-8 is that core mesh size of 0.5mm is fine enough to capture the flow field of the infinite bundle. The adequacy of the chosen boundary layer mesh and wall treatment cannot be checked in the infinite bundle geometry, but only by comparing the simulation results to the experiments available. However, it is expected that all y+ wall treatment should be the best suited for the present benchmark exercise due to the complicated nature of the flow along the vanes, e.g. boundary layer separation. The chosen uniform mesh size of 0.5mm is not expected to be the optimal in terms of grid efficiency. Gradient adaption would probably result in more efficient, less time consuming computations but these are not explored in this work.

6.2 Assessment against Existing Literature Containing Cutout Vanes

6.2.1 Reference Results

Grid sensitivity studies have also been conducted for the full geometry reported by KAERI [1, 2] in order to verify the effect of the outer walls and bundle housing on the flow field, as well as the integrated behaviour across all subchannels. In this case, however, only 1 and 0.5mm meshes were examined since the computational effort for a 0.25mm base grid was exceptionally large. Running the full geometry of the experiment made it possible to compare the simulation results with the experimental ones. Figure 9 presents average streamwise and spanwise velocities for the two meshes along with the experimental results. Due to the fact that results for the two meshes differ from each other, it is concluded that the mesh of 0.5mm should be used for the final submission. Simulation with mesh of 0.25mm of this domain was not possible within the computational resources available at this time. The blue shaded regions on the graphs of Figure 9 show the location of the possible effect of the cutouts geometry. As it was mentioned previously, the exact geometry of the cutout section of the vane was not reported in detail. Hence, one could expect that the results are sensitive to the exact cutouts form and size.

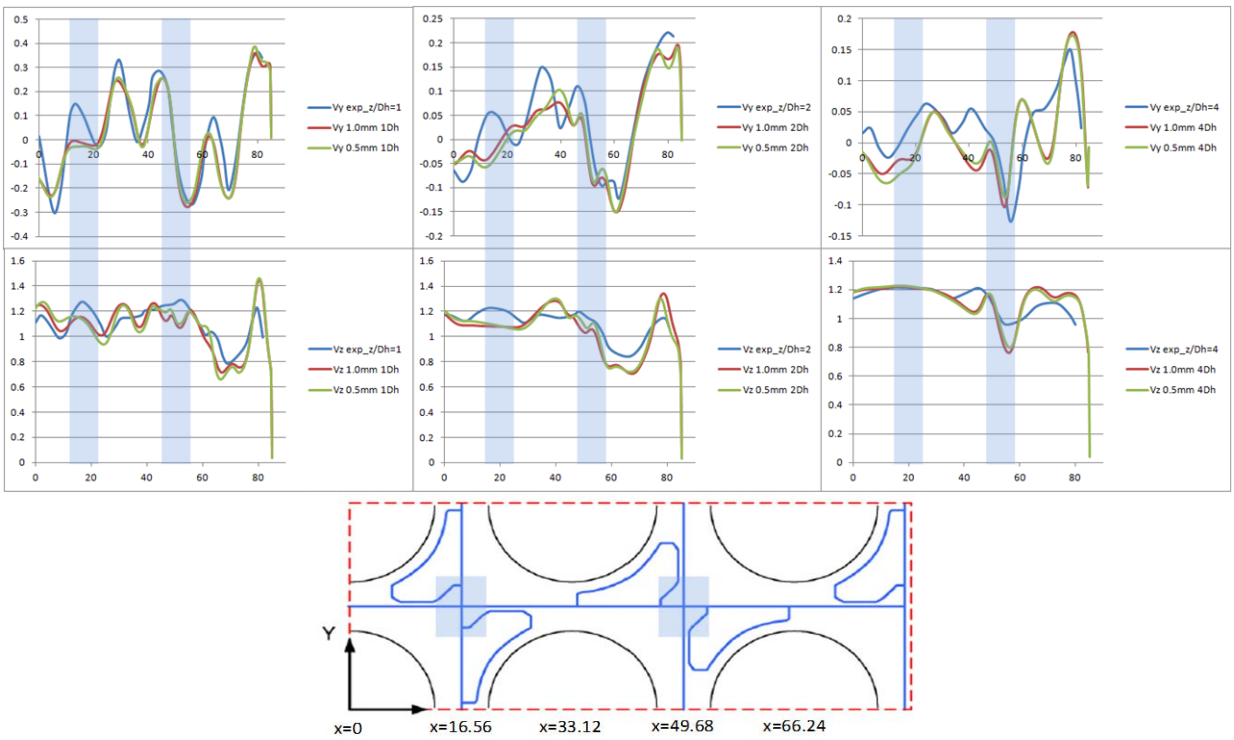

Figure 9. Grid size sensitivity for the KAERI 2008 experiments. Average velocities.

Figure 10 presents the rms values of the three velocity components. As the realizable k-ε model was employed for the reported simulations, Boussinesq assumptions of the proportionality of the Reynolds stresses to the average velocity gradients are used to reconstruct the spatial stresses. Though the model does not solve explicitly for the Reynolds stresses, their values were recovered in the postprocessing. The rms values presented are the square roots of the normal Reynolds stresses. It has to be noted that one of the features of the realizable k-ε model is the positiveness of the normal Reynolds stresses which is not always assured using other 2-eq models counterparts.

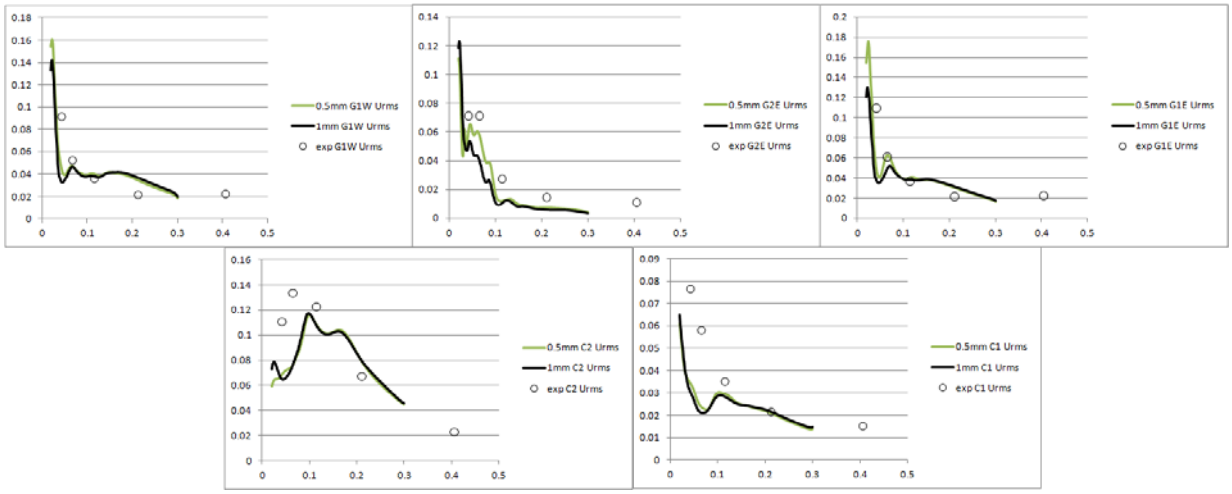

Figure 10a. Grid size sensitivity for the KAERI 2008 experiments. Urms.

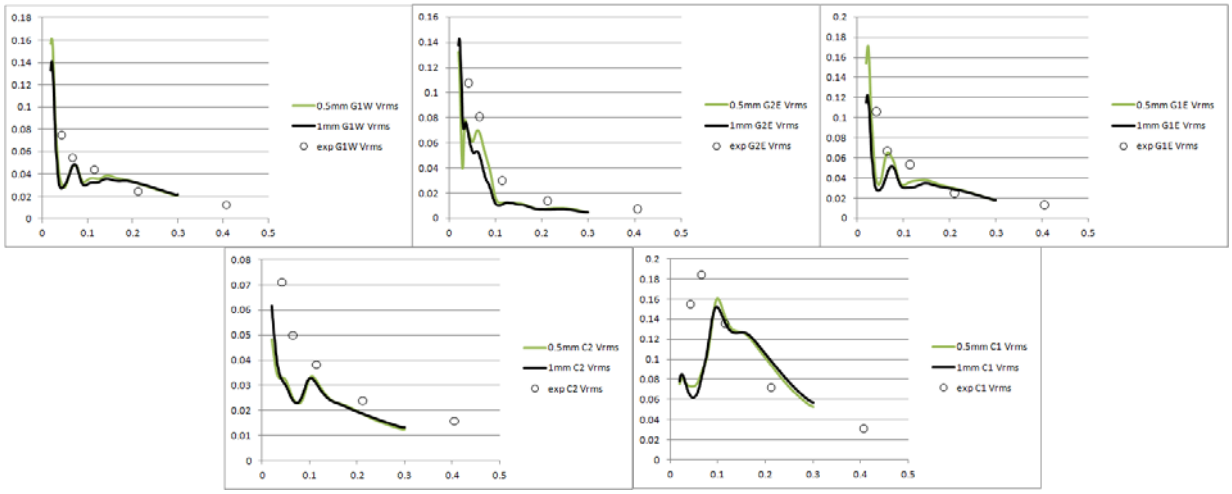

Figure 10b. Grid size sensitivity for the KAERI 2008 experiments. Vrms.

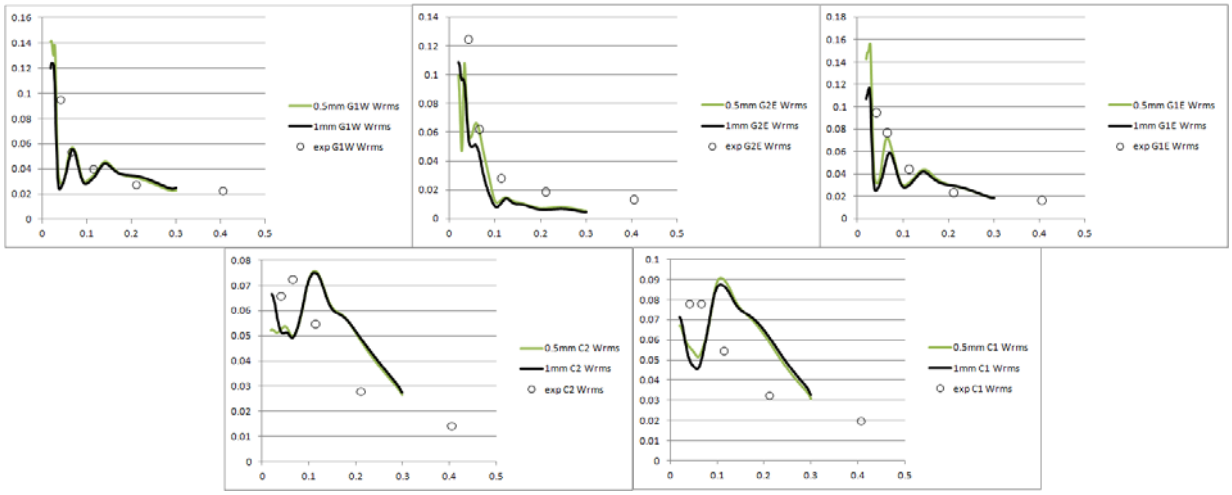

Figure 10c. Grid size sensitivity for the KAERI 2008 experiments. Wrms.

As in the case of the average velocities, the results of the rms values show some differences for the finer mesh. It also has to be mentioned that the most difference between the simulated and the experimental results are observed along the lines C1 and C2 that run from the regions of the vane cutouts – once again a geometry effect can be assumed. Figure 11 presents the contours of the two spanwise rms velocity components at the streamwise distance of four hydraulic diameters from the vanes tips – the only ones reported in the papers [1, 2].

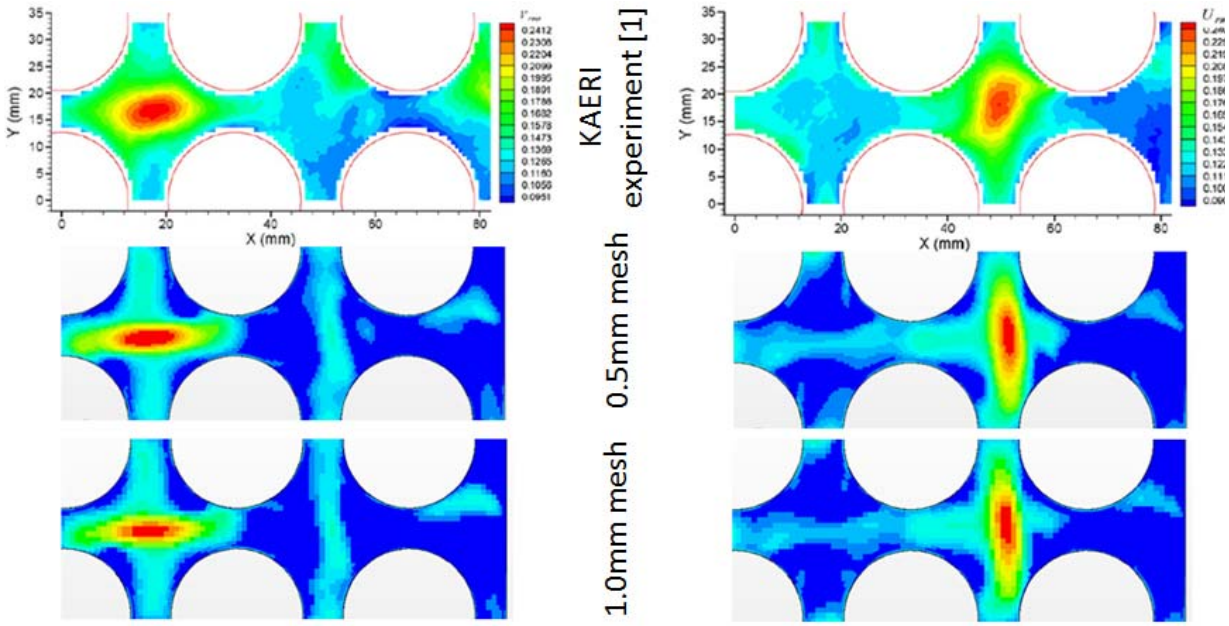

Figure 11. Grid size sensitivity for the KAERI 2008 experiments. Urms and Vrms at z=4Dh.

It has to be noted that Figure 11 shows there are regions where the predictions of the model used in the present study differ quantitatively, e.g. near the bundle wall (the far right part of the contour maps). On the other hand, both the location and the values of the maximums in Urms and Vrms values are predicted acceptably by the model. Here, no appreciable differences were found in the results of both meshes used.

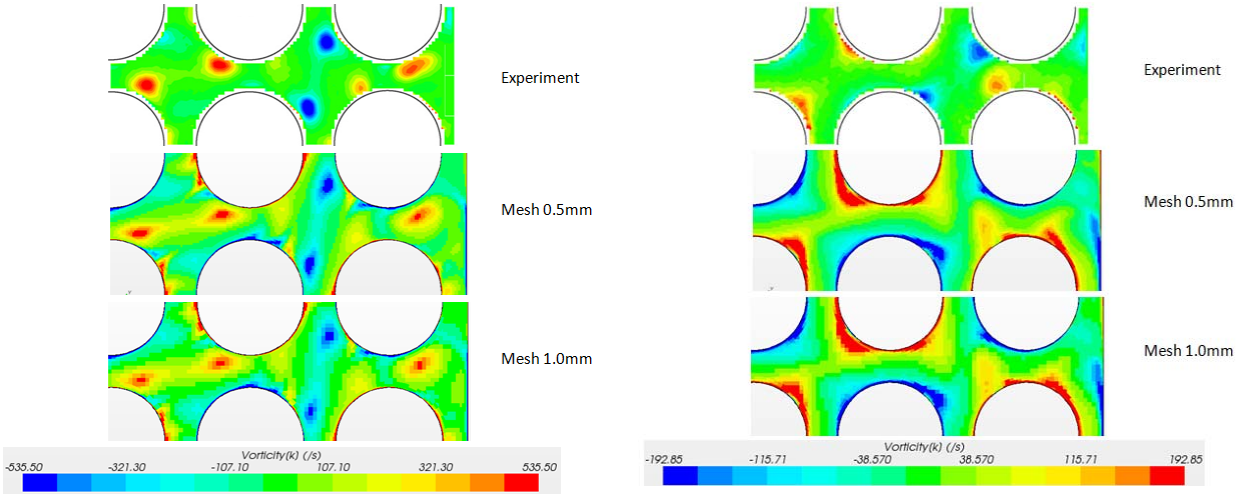

Figure 12. Grid size sensitivity for the KAERI 2008 experiments. Streamwise vorticity contours for z=1Dh (left) and z=4Dh (right).

Vorticity contours presented in Figure 12 suggest that this flow field characteristic at z=1Dh is captured quite good by the model for the two meshes presented. The contours at z=4Dh are quite different for the model and the reported measured values in particular close to the rod walls. It has to be noted that these regions are difficult to measure and the reliability of the experimental results here is questionable. Nevertheless, in the view of the relative success of the predictions at z=1Dh, it can not be concluded that the contours for z=4Dh and downstream are expected to be as good as those close to the vane tips in the final benchmark experiment simulation. It can be concluded that 0.5mm mesh should be used for the final submission.

6.2.2 Inlet Velocity Profile

The information provided by the benchmark organizers concerning the inlet boundary conditions was not sufficiently detailed to reconstruct the full and accurate upstream boundary condition for the CFD simulations of the benchmark geometry. Rather than using the experimentally measured (but sparse) upstream velocities as a boundary condition we developed our own profiles and performed qualitative checks against the limited upstream measured data. In order to generate our own velocity and turbulence boundary conditions we conducted several studies of flow development upstream of the turbulent grid structure. Here we proceeded to increase the development length in the simulations until fully developed flow at the inlet of the grid structure was obtained. This method was consistent with most other participants in the benchmark and the results agreed qualitatively with the available measurements.

As was mentioned in section 6.1.2, centralizing buttons were found to be the only reason for the solution instability. Hence a coarse mesh was used within the spacer region, upstream of the mixing vanes, in order to filter out those instabilities. The walls of the spacer grid, the buttons and the rod walls were meshed in such a manner as to result in y+ values between 30 and 80. This assured appropriate boundary layer modelling for the all y+ wall treatment. The bare rods flow development section was meshed in the same manner as the spacer grid. The mesh used is presented in Figure 13, in accordance with the wall function specifications.

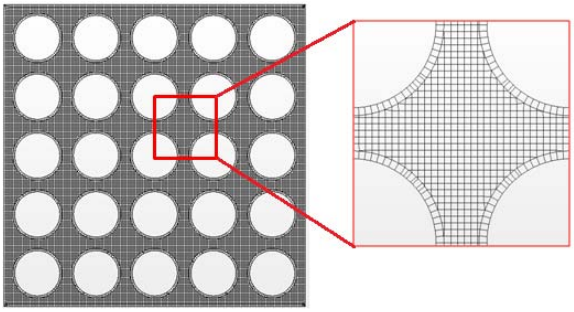

Figure 13. Bare rods flow development region grid.

The simulations of a bare 5x5 rod bundle have shown that the RSM models resulted in the closest to measured flow profile for this geometry. However, based on the results in the preceding sections the realizable k-ε outperforms the RSM model in the region downstream of the spacer grid – see Figure 14.

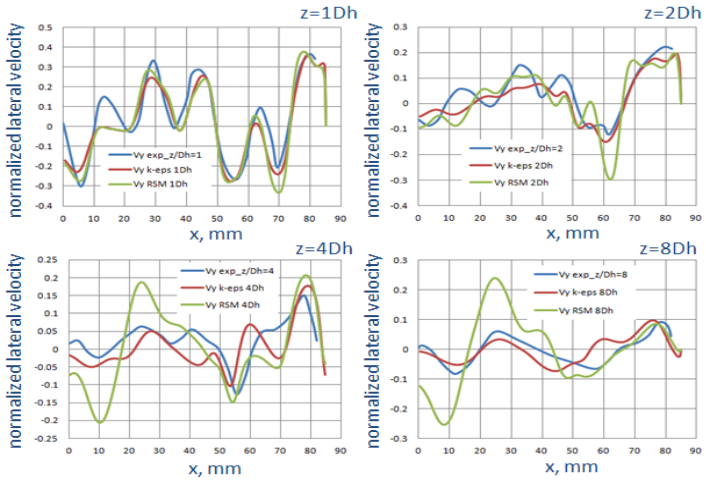

Figure 14. Realizable k-ε vs RSM in the infinite bundle test case

As the spacer grid has a considerable impact on the flow field, it was decided to use realizable k-ε throughout the entire computational domain. In our model we have increased the upstream bare rod bundle length until fully developed conditions were reached prior to the spacer grid. The development length was about 80 hydraulic diameters long – see Figure 15.

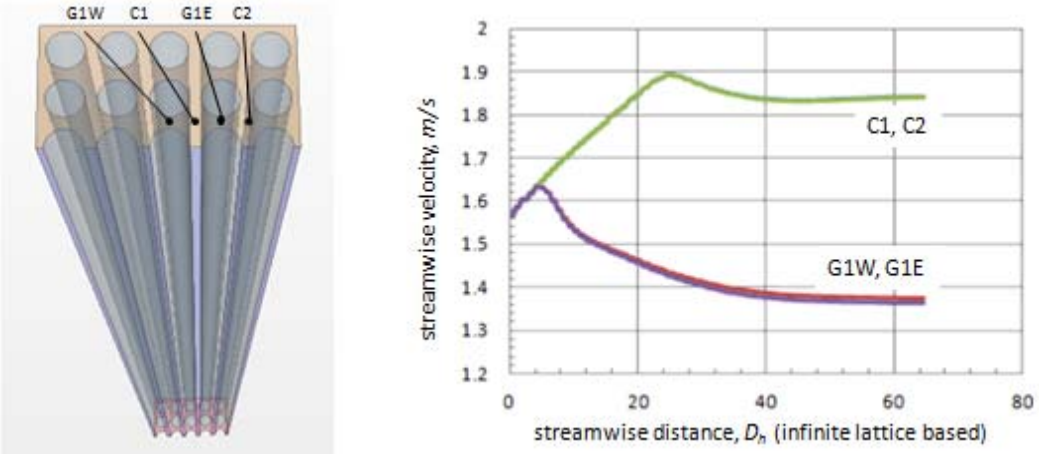

Figure 15. Flow development in the bare rods bundle.

As steady realizable k-ε model was used in this coarse meshed region, there was no appreciable calculation time penalty comparing to the case where the flow could be developed in a separate calculation and only the flow outlet profile used subsequently as an inlet to the spacer grid. The method of flow development was consistent with most other participants in the benchmark.

6.2.3 Effect of Symmetry

Although it is understood that due to the non-uniform power generation in the real fuel bundle, geometrical symmetry of the flow field for the isothermal case will not hold for the heated channel, it is thought to be advantageous to use the symmetry for cutting down simulation time and to allow for the finer meshing to be applied for verification[5]. Figure 16 presents the applied symmetry conditions for the split and the swirl vaned grids.

[5] It should also be mentioned that for unsteady simulations symmetry should not be imposed in any way since it may violate the physical phenomena such as alternating vortex shedding, which are out of phase on different sides of the symmetry plane.

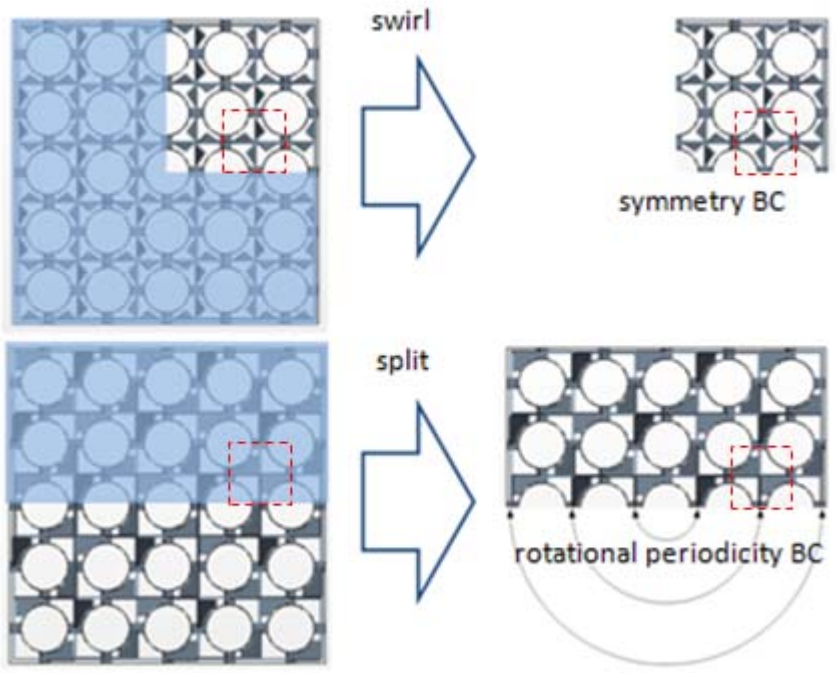

Figure 16. Periodic BC for the split (right) and symmetry for the swirl (left) grids.

Only the results where the most differences between the full and the partial geometries were observed will be presented – see Figure 17.

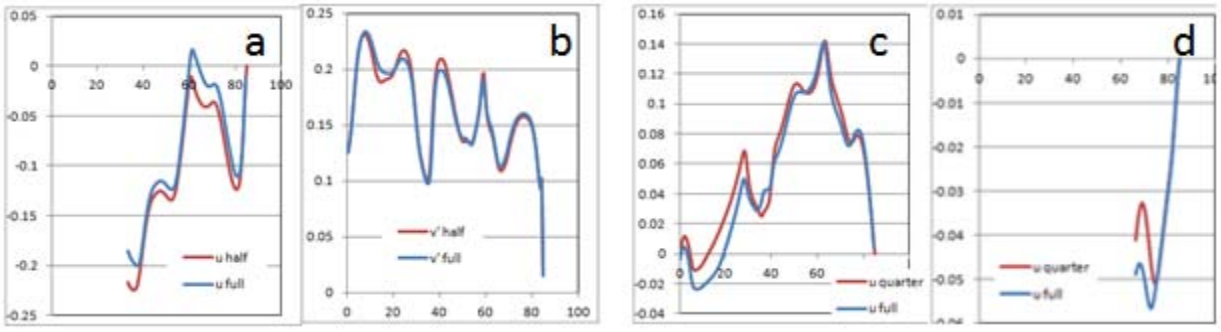

Figure 17. Full and partial geometry comparison. a) split vanes, *u* velocity, z=10Dh, $y=y_2$, b) split vanes, *v'* velocity, z=4Dh, $y=y_1$, c) swirl vanes, *u* velocity, z=10Dh, $y=y_1$, d) swirl vanes, *u'* velocity, z=10Dh, $y=y_3$

Figure 18 presents the vorticity integrals for the four cases as it should be submitted in accordance with the benchmark specifications.

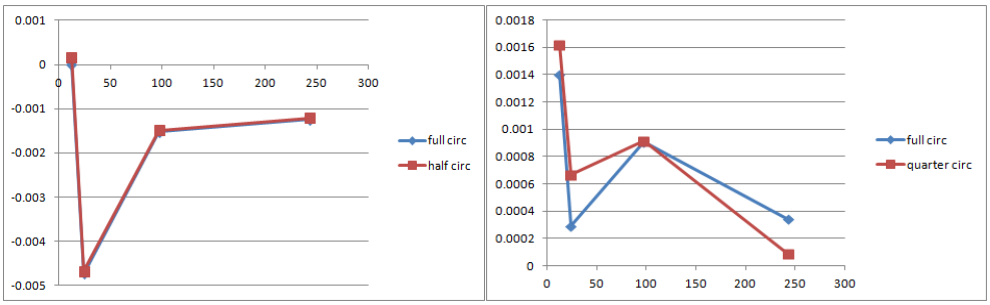

Figure 18. Circulation for split (left) and swirl (right) grids.

It is seen that the most differences are observed in the case of swirl grid, especially in the circulation values at 1 and 10 hydraulic diameters downstream of the vanes tips. On the other hand, the vorticity contours presented in Figure 19 look quite similar for all the axial positions required for submission, even for the swirl grid.

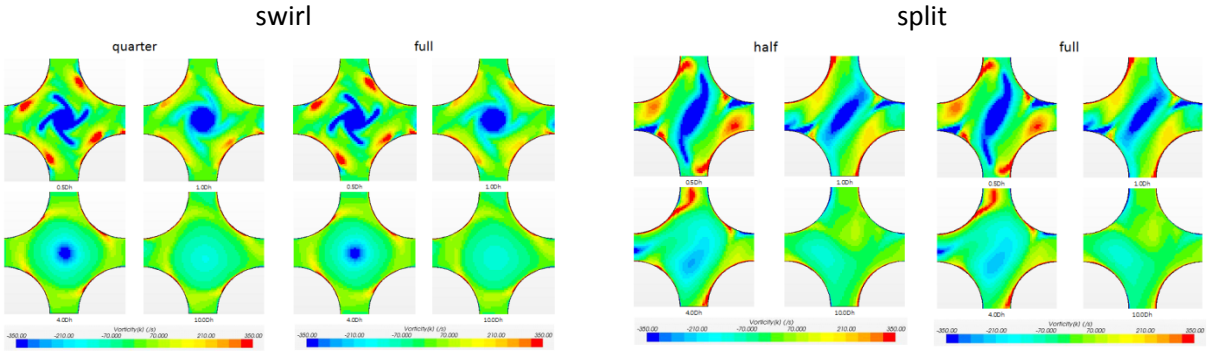

Figure 19. Vorticity contours.

Based on the apparent sensitivity of some values in the swirl-case to symmetry representation, it was decided to submit the results of the full geometry simulations for both swirl and split grids for consistency.

6.2.4 Outlet Plenum Effects

All the presented results of the flow field in the KAERI 2008 experiment were simulated with the calculation domain extended about 0.5m downstream of the final "measuring" plane. This approach while convenient for mesh construction, differs substantially from the one that is used in the benchmark experiment, and probably from the one used in 2008. During the experiments in the benchmark setup, the vaned grid was moved in the way that the distance from the measurment plane downstream to the changes in the bundle crossection was always held consatant and equal to 10mm. Strarting from this position the rods diameters were gradually reduced and then the flow entered the outlet plenum. The flow exits the test section through three oultet pipes the plenum. Figure 20 presents the geometry simulated in order to find out if the effect of this downstream geometry could have an appretiable impact on the measurements. Measurements of the plane situated at z=0.5Dh was simulated due the lowest possible domain size in this case. Due to the large size of the plenum and an attempt to filter out the anticipated transient behavior in spliting the practically rectangular flow from the bundle to the

three equally azymuthaly separated directions, coarse core mesh was empoyed in the plenum. Nonetheless, the grid size was still larger than acceptable for the relatively quick simulation time, thus, the core mesh in the bundle was also increased from the value of 0.5mm to 1mm.

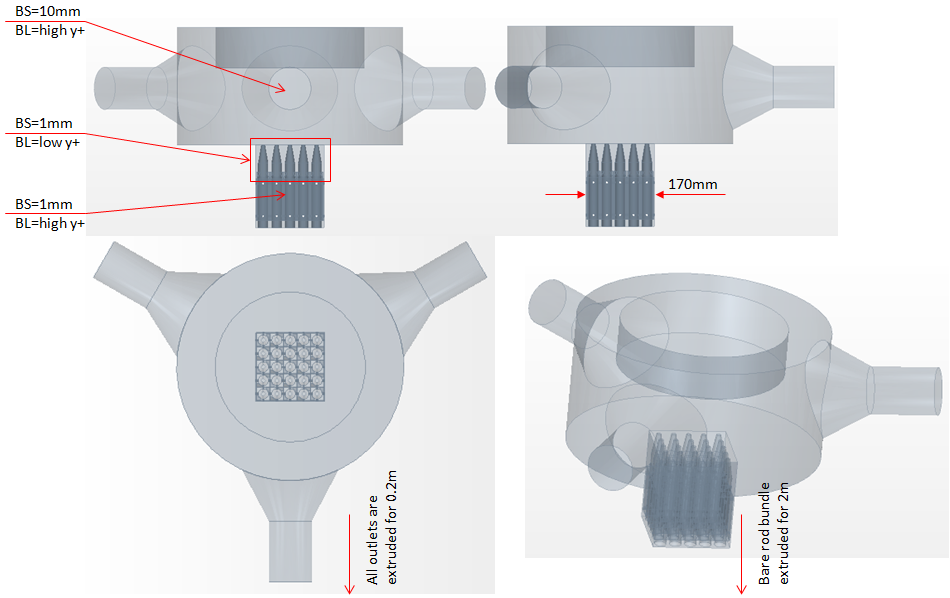

Figure 20. The outlet plenum impact. The computation domain and grid definition.

Results presented in Figures 21 and 22 suggest that in the limits of the model used, the impact of the outlet plenum is expected to be negligible.

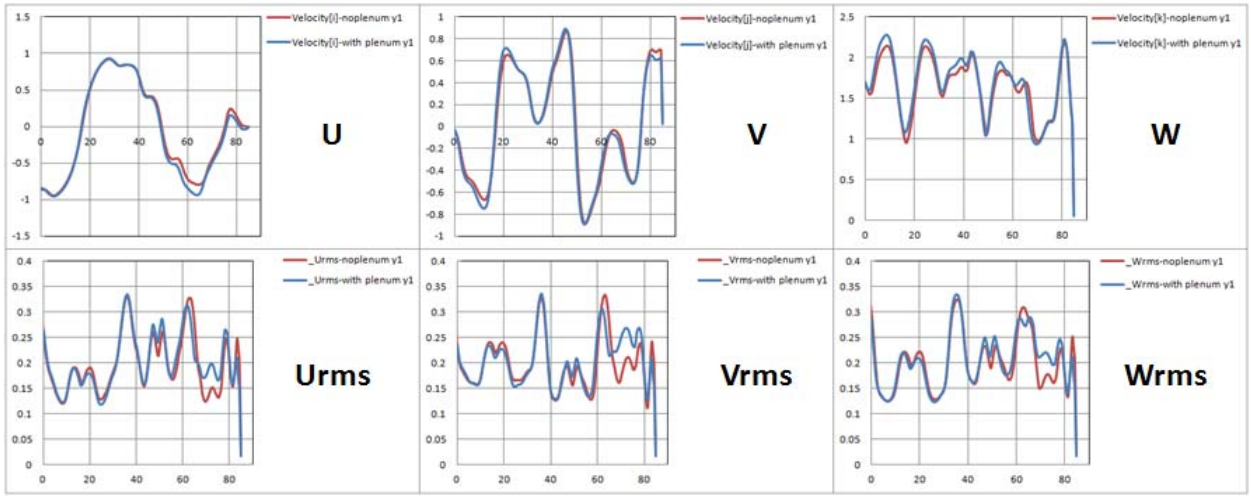

Figure 21. The outlet plenum impact. Average and rms velocities.

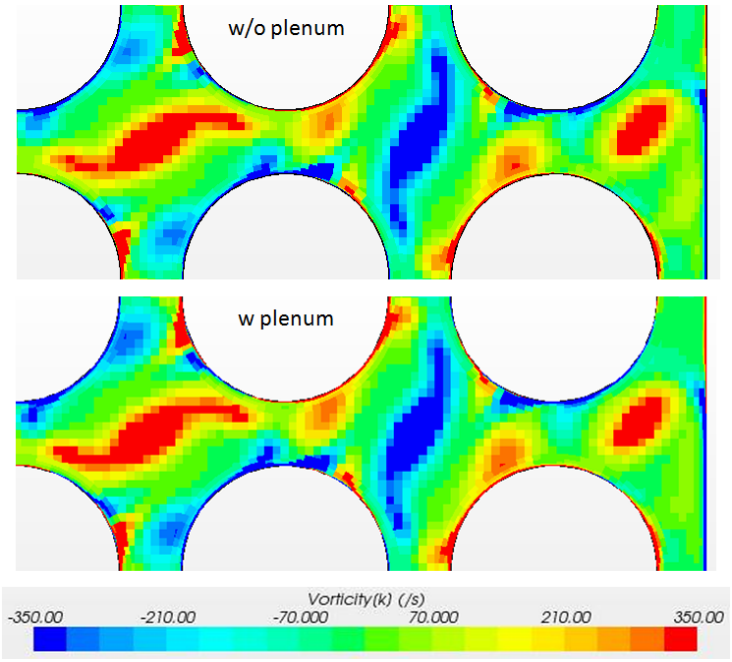

Figure 22. The outlet plenum impact. Vorticity contours.

As it was mentioned above, the grid size in the bundle had to be coarser than the size verified in our comparison to the KAERI experiments of 2008: 1mm instead of 0.5mm. Figure 23 presents the computation domain where this grid coarsening was not necessary due to the smaller geometry simulated. Only the impact of the rods diameters reduction could be checked in this case.

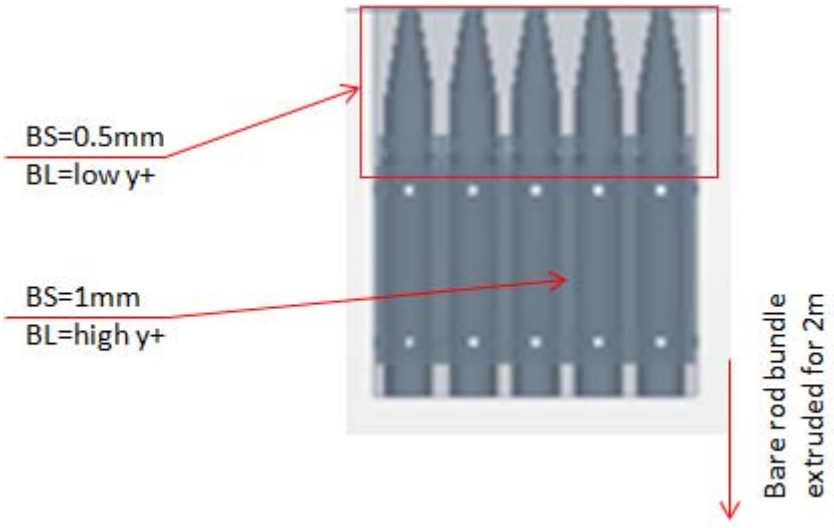

Figure 23. Rod diameter tapering impact. Computational domain and grid characteristics.

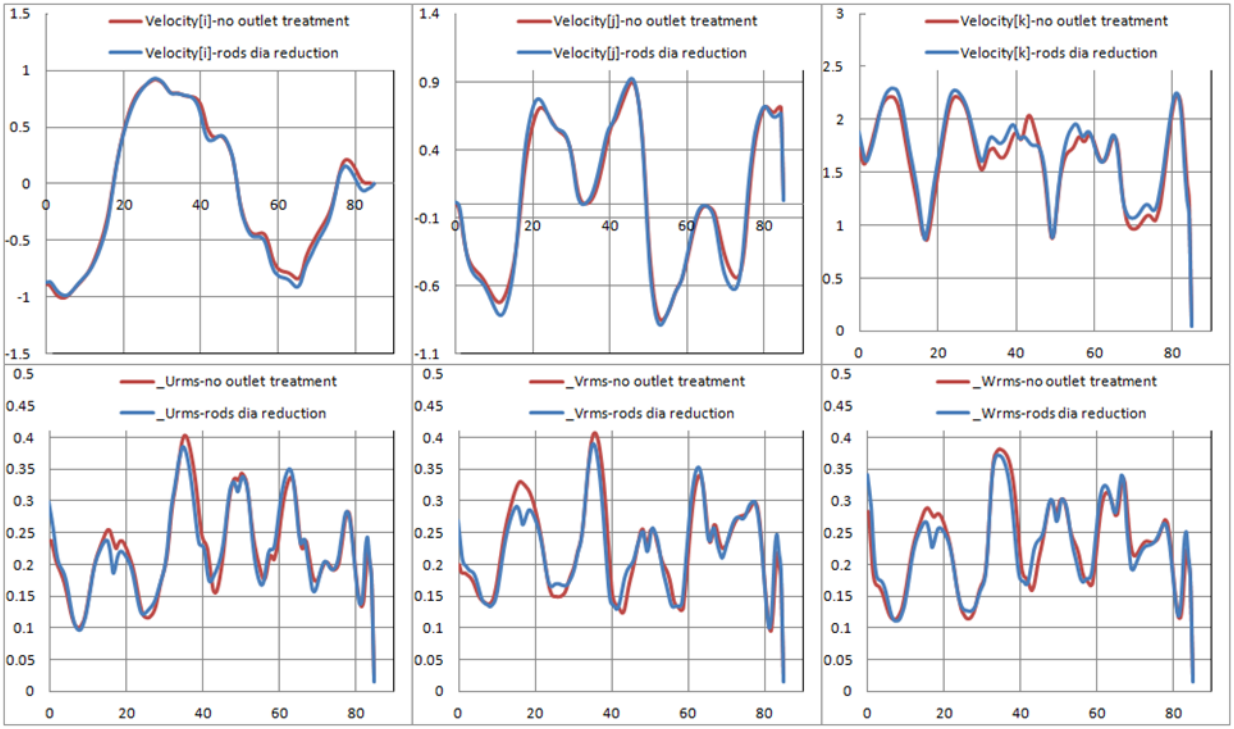

Figure 24. Rod diameter tapering impact. Average and rms velocities

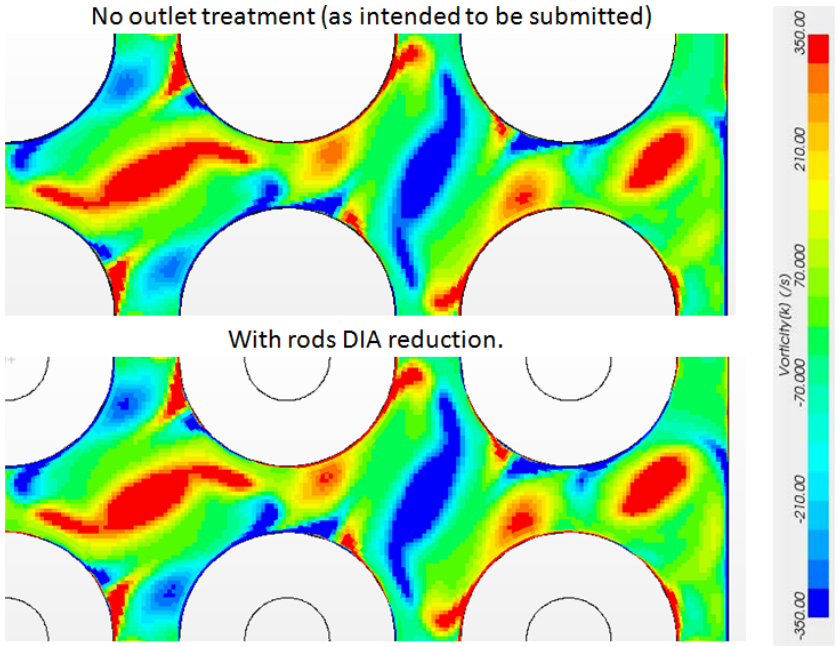

Figure 25. Rods diameters reduction impact. Vorticity contours at z=0.5Dh.

As in the case of the whole plenum simulations, the effect of rods diameters reduction was found negligible for the case of the fine mesh used for this study – see Figures 24 and 25. It can be concluded

that one could expect no appreciable impact of the outlet geometry on the measurements results in the benchmark experimental setup.

6.2.5 Effect of Cut-out Geometry Assumptions

As it was mentioned, the exact geometry of the vanes and cutouts is not reported in KAERI papers [1,2]. Hence, an attempt was made to assess the sensitivity of the simulation results to the geometry of the vanes cutouts. Two sizes were used as it is depicted in Figure 26, but the literature did not give sufficient details on their size and profile. Ideally, this information would have allowed for a more thorough investigation of models, however, in light of the missing information we have examined the effect of cutouts only since it was believed that they most significantly affect the flow field. Figure 27 present the average velocities in *y* and *z* directions at the locations z=1,2,4 and 8Dh downstream of the mixing vanes tips. Figure 28 presents the rms values of the two cutout geometries as they are compared to the results of the experiments reported by KAERI. Figure 26 presents comparison of the vorticity contours.

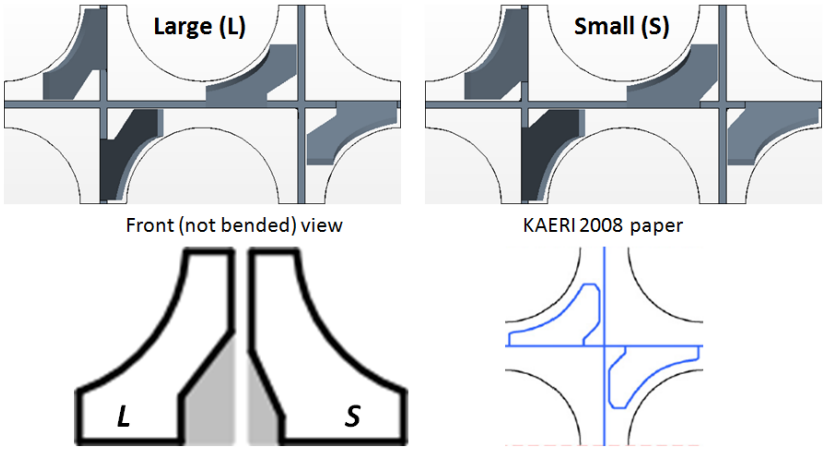

Figure 26. Cutout geometry.

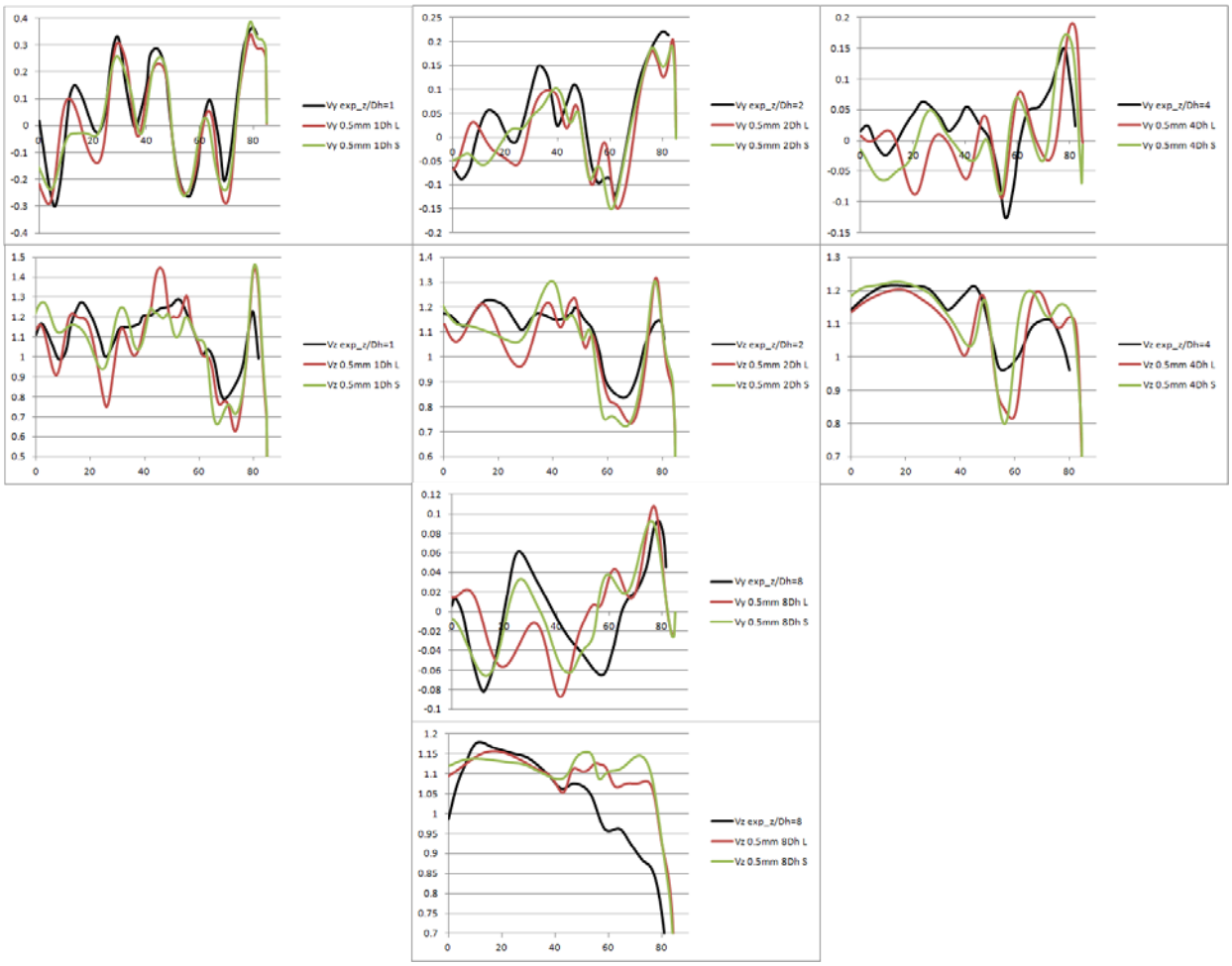

Figure 27. Cutout geometry effect. Average velocities.

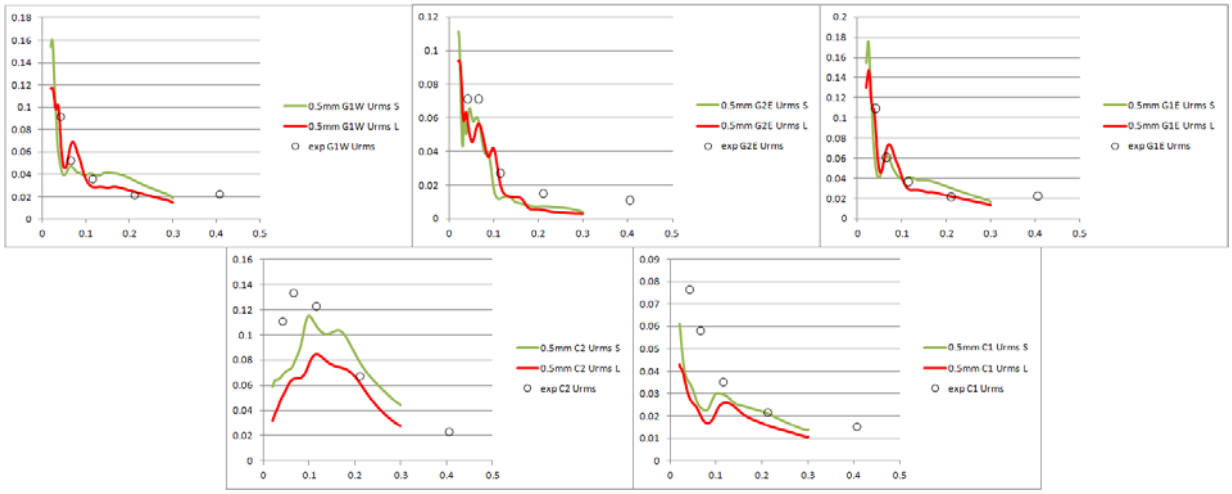

Figure 28a. Cutout geometry effect. U_{rms}.

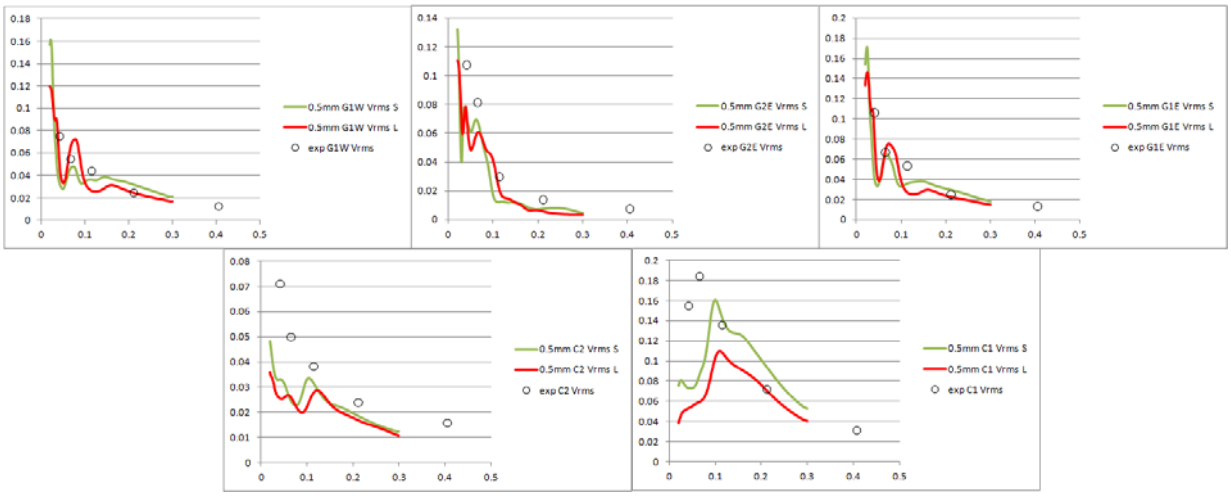

Figure 28b. Cutout geometry effect. V_{rms}.

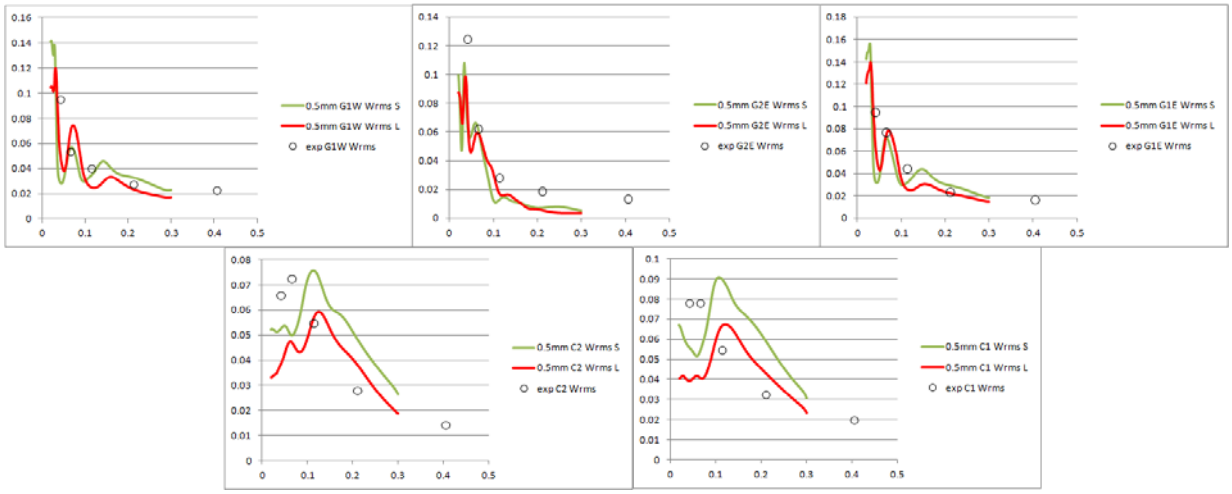

Figure 28c. Cutout geometry effect. W_{rms}.

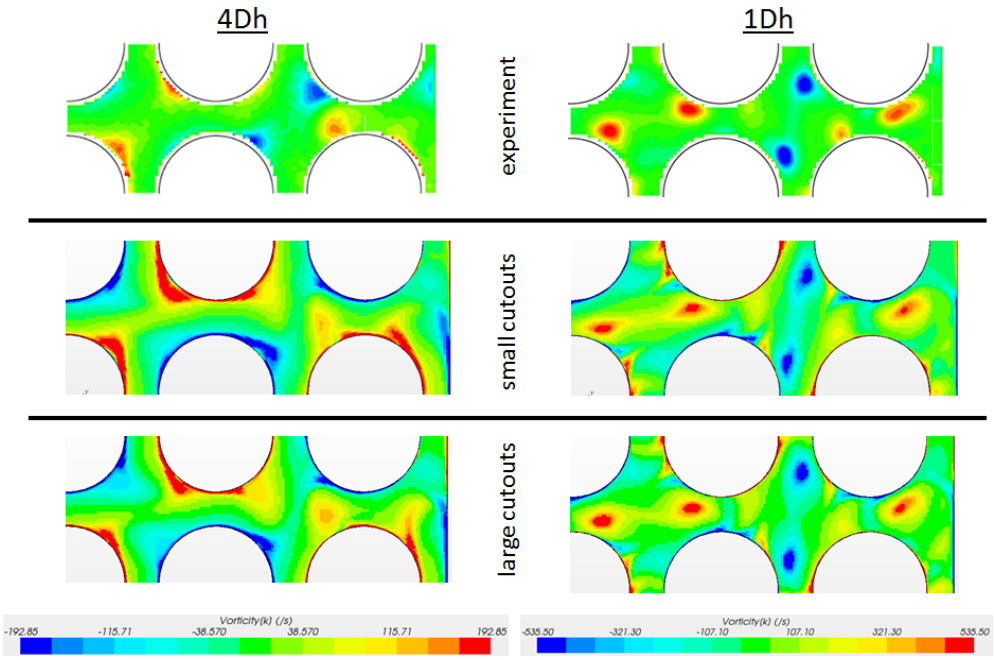

Figure 29. Cutout geometry effect. Vorticity contours.

Results presented in Figures 27-29 suggest that the flow field is sensitive to the cutout geometry and one could expect that if other geometrical features are not modeled in the exact manner, it could also impact the simulation results. No definite conclusion can be drawn concerning the choice out of the two geometries studied.

7 RESULTS OF THE 2012 OECD-NEA BENCHMARK SIMULATIONS

As it was announced at the benchmark conclusion meeting at CFD4NRS, that out of the results at four different streamwise locations and three spanwise positioned lines, only the results at 1Dh and 4Dh at one spanwise located line would be compared[13]. The results at z=1Dh and z=4Dh for split and swirl vaned grids are presented in Figures 30 and 31 respectively.

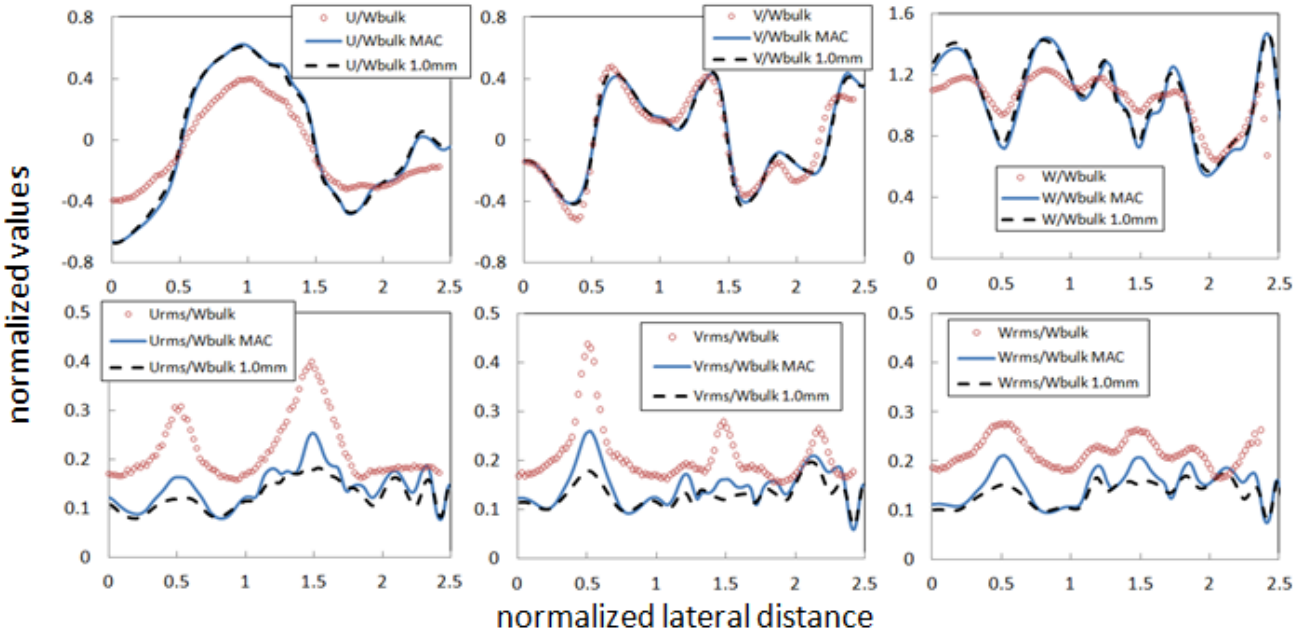

Figure 30a. Split vanes results at 1Dh as submitted. Comparison with the experiment.

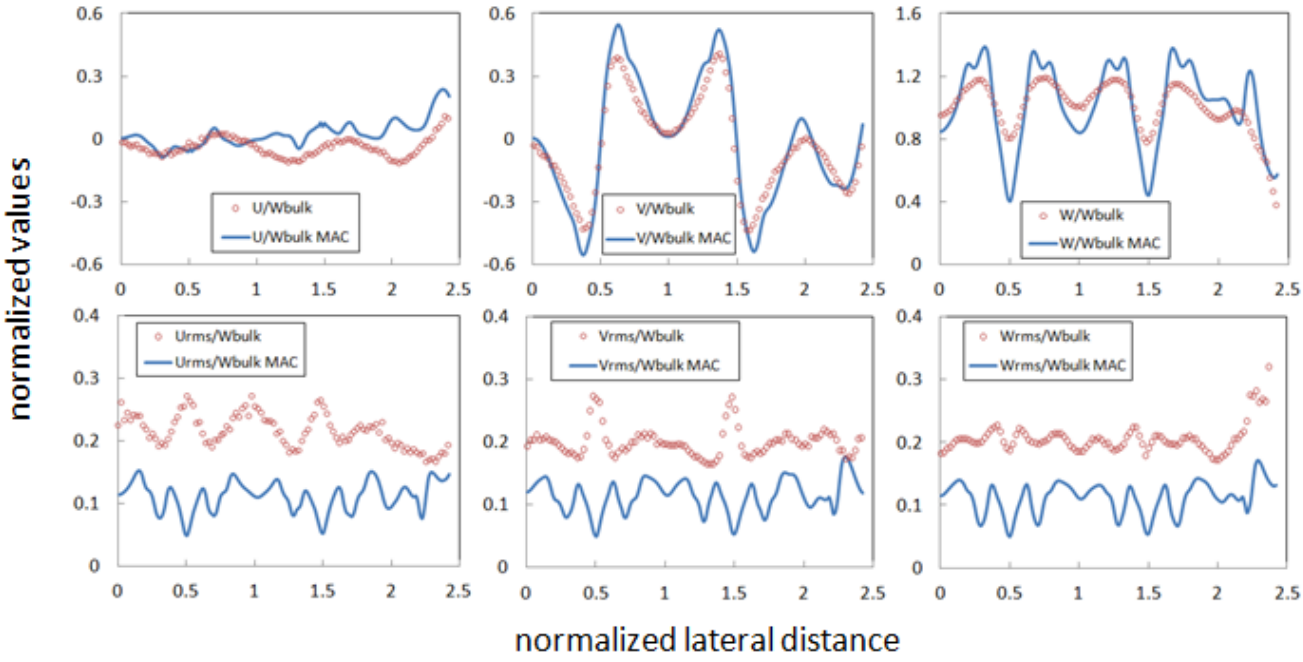

Figure 30b. Swirl vanes results at 1Dh as submitted. Comparison with the experiments.

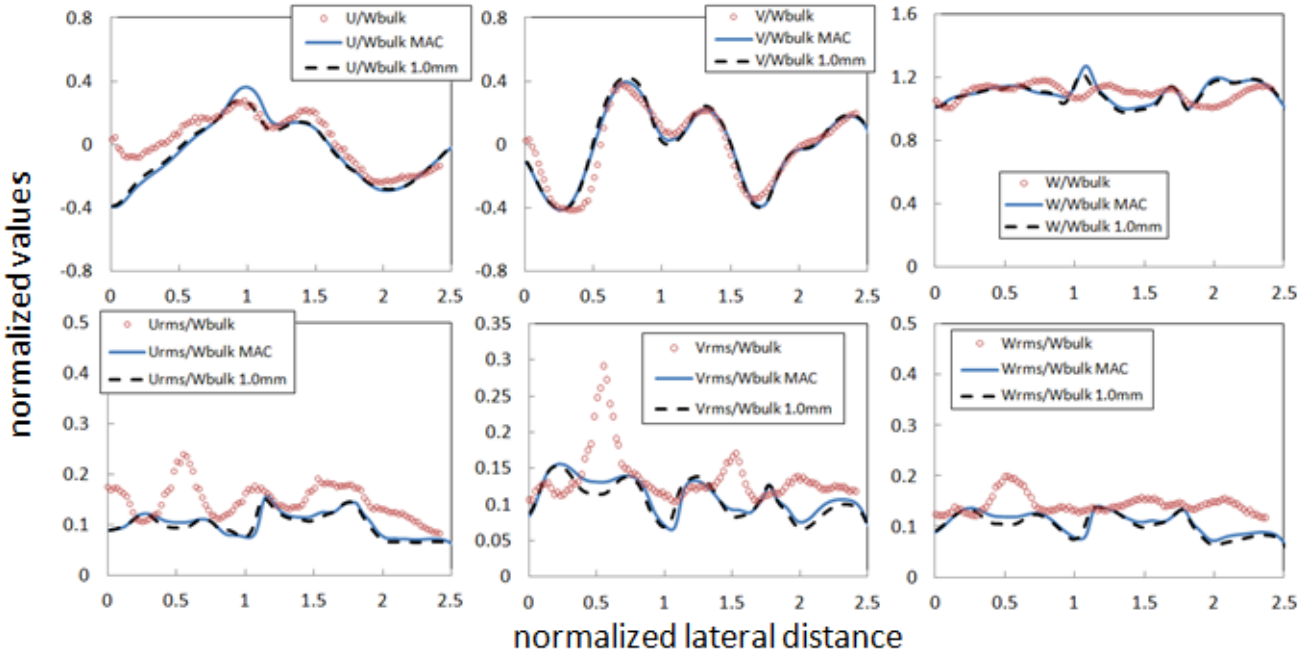

Figure 31a. Split vanes results at 4Dh as submitted. Comparison with the experiment.

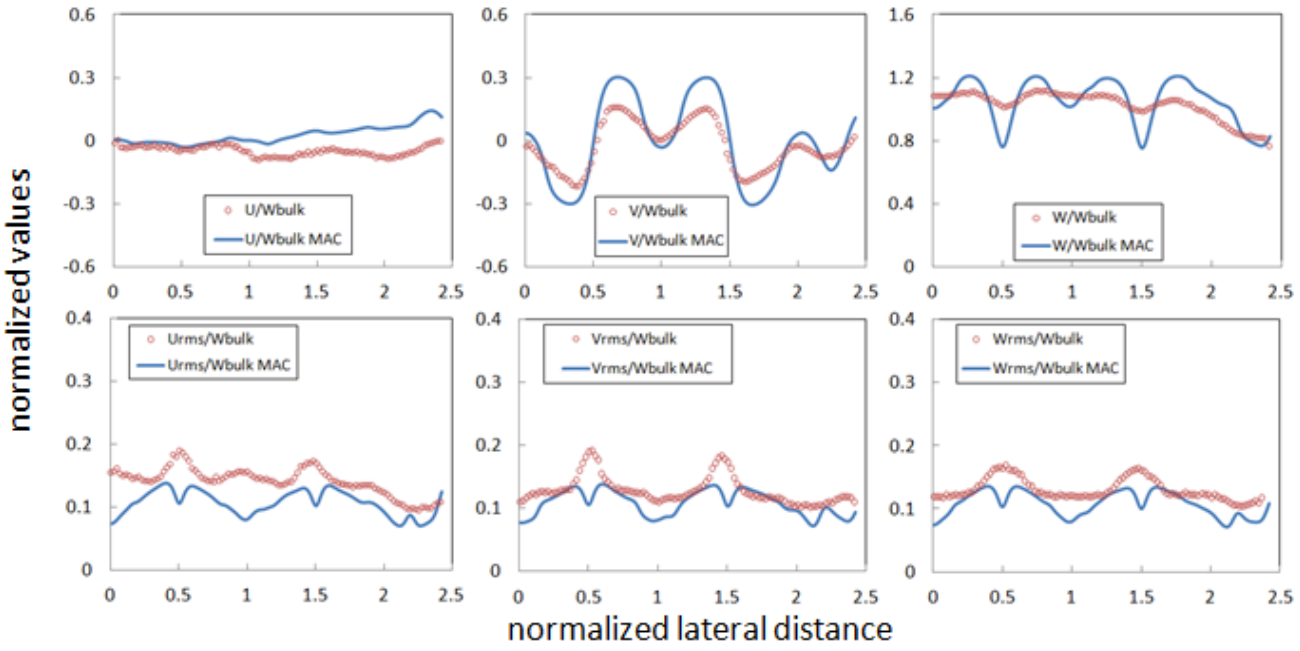

Figure 31b. Swirl vanes results at 4Dh as compared to experiment.

It can be generally concluded that the results for the split vanes fit better to the experiments than those of the swirl vanes. As a high level observation the maximum and minimums of the profiles are over- and under predicted respectively, exaggerating the flow profiles as compared to the experimental measurements. The rms values are generally under predicted near the vanes and are comparable with

the measured values magnitude at the far downstream location of four hydraulic diameters. Taken together it can be generally concluded that the level of turbulence in the simulations was under-predicted as compared to the experiment (possibly from the large scale meshing used to supress vortices from the positioning buttons).

Figures 30a and 31a presents additional results of split vanes for the coarser grid, 1.0mm instead of submitted 0.5mm core mesh with the same boundary layer. In case of 1mm core mesh, the computational cells number is about five times less than that for the submitted 0.5mm mesh: 13 instead of 60M cells. This means that the computational time could be cut by approximately a factor of five. Usual calculations with 60M cells for both split and swirl grids took about 30 hours clock time per case on a computer system containing 32 processors (2GHz x86-64 CPU) with 64 GB of memory, running under Linux (Centos 5.5, kernel version 2.6.18)

It is seen that using a coarser grid does not generally affect the average velocity values predicted. On the other hand, the rms values, especially close to the grid are significantly under predicted with the coarser mesh. In some of the cases, the average velocities are better predicted with a coarser grid (e.g. U velocity at 4Dh – see Figure 30a top left), but it is by no means justified to use it as it does not satisfy the mesh convergence criteria.

To get a more complete picture of the comparison of the rms velocity values, Figure 32 presents the U_{rms} maps as were measured at the distance of 1Dh from the vane tips of the split type grid along with its submitted counterpart. The black dash line presents the line along which the results were submitted – see the left bottom graph in Figure 30a above.

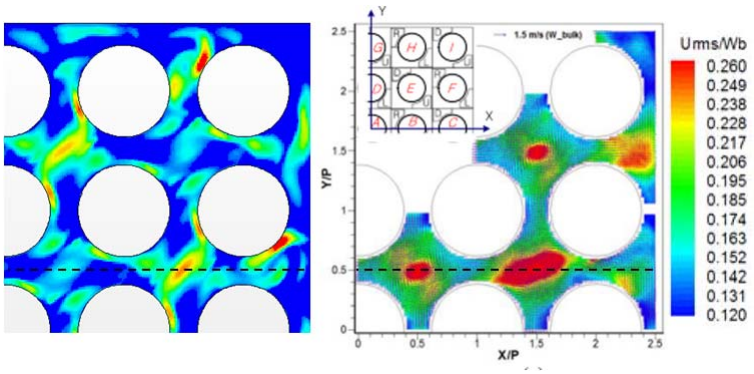

Figure 32. Urms values at 1Dh for split type grid

As it was expected from the comparison presented in the previous section for the 2008 KAERI experiments [1, 2], while the location of the minima and maxima of the rms values are mostly predicted correctly, the absolute values are under predicted by the steady RANS model used.

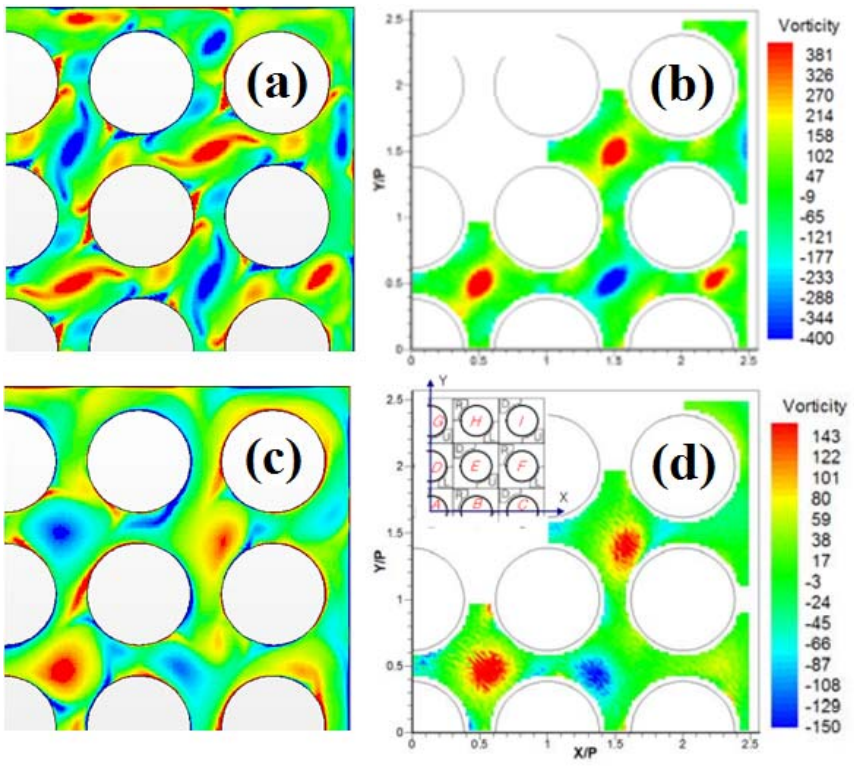

Figure 33. Vorticity contours for split vanes - comparison with experiments. (a) 0.5Dh calculations, (b) 0.5Dh measurements, (c) 10Dh calculations, (d) 10Dh measurements.

Figure 33 presents comparisons of the calculated and measured contours of streamwise vorticity. Measured values close to the rods are absent due to the experimental difficulties in this region. While some small differences exist, both qualitatively and quantitatively the simulations succeeded in predicting the vorticity.

One of the important criteria for the effectiveness of the mixing vane grid is its ability to maintain high values of vorticity as far downstream as possible. This can be further related to the heat transfer enhancement. Participants were asked to submit the streamwise vorticity (ω_z) integral (circulation, Γ) over one subchannel area at four downstream locations:

$$\omega_z = \frac{\partial v}{\partial x} - \frac{\partial u}{\partial y}$$

$$\Gamma = \iint_{subchannel} \omega_z \, dA$$

The predicted circulation as a function of position from the grid is shown in Figure 34b. Due to the difficulties in measuring the velocity components close to the rod walls, a thin strip was excluded from the vorticity integral required for submission. The comparison of the submitted circulation values with the measured ones for both grids is presented in Figure 34b.

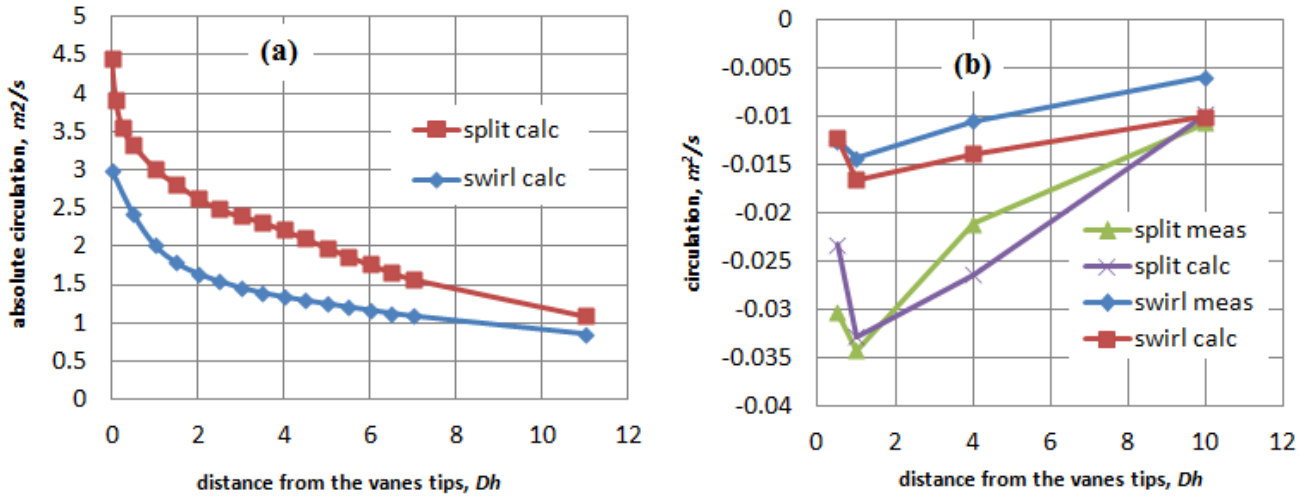

Figure 34 a) Absolute circulation as a function of downstream positions. b) circulation as a function of downstream positions

As in the case of the average velocity values, the circulation is predicted better for the case of the split vanes. It can also be seen that although the higher circulation values are those for the split vaned grid than for the swirl one, its decrease with downstream distance is also higher as it was predicted numerically.

As it is seen from Figure 34b, the streamwise vorticity integral (circulation) as it was defined in the benchmark specifications behaves non-monotonically. Absolute value of the circulation could be suggested as an alternative comparison method:

$$\Gamma = \iint_{total\ cross-section} |\omega_z| dA$$

Integration over the entire bundle cross section (not one subchannel) as an indication of the total, integral effect of the grid was considered. The results for both grids are presented in Figure 34a. It showed a monotonous decay with a streamwise distance from the mixing vanes for both swirl and split cases towards its asymptotic value of the bare rod bundle.

8 CONCLUSIONS

The objective of this report was to document the results of the CNSC sponsored research on CFD applications in rod bundle geometry flows. Specifically this report outlines the rationale behind

choosing the calculation scheme for the final submission and presents a comparison of the submitted results to measurements of OECD/NEA co-organized MATiS-H experiments.

First, the methodology used to examine the predicted flows within the grid spacer and through the mixing vane tips is presented. It includes the separate effect studies that were performed on small scale geometry domains. This allowed the use of fine mesh resolution and transient calculations in order to quantify the potential impact of different flow features on the final result. In particular we focused our studies on the potential unsteady behaviour generated from the positioning buttons and the vane tips. From this examination it was concluded that we would adopt a coarse grid structure in the vicinity of the buttons such that potential unsteadiness would be filtered. This had the benefit of allowing 2-equation steady-models to converge with minimal CPU expense, and hence met the overall objectives of obtaining a solution within reasonable time-frames. However, such assumptions may have damped the bulk turbulence levels somewhat, and this was observed in the comparisons to the final benchmark where it appeared that there was a steady offset in our RMS velocity values.

Based on the studies of partial geometries, the numerical approach was finalized to be used in the calculations of the benchmark geometries. Steady, realizable k-ε model as incorporated in the commercial CFD STAR-CCM+ software was employed for the final submission. Again, the choice of the model was mainly dictated by the desire to obtain a reasonably accurate solution with a minimal number of nodes and appropriate turbulence models such that the results would be engineering relevant (i.e. capable of adding in heat transfer effects as would be needed in industrial CFD application). Our examination of outlet geometry effects demonstrated that they do not play a significant role in the end benchmark prediction results.

The comparison with the experimental results has revealed that the results for the split vanes fit better to experiment than those of the swirl vanes. The overall conclusion for most of the average velocity profiles is that their local extrema are over predicted by the model used. Consistent with these results, was that the rms values are generally under predicted near the vanes and are of a comparable magnitude at the far downstream location of four hydraulic diameters. Hence these observations indicate that the bulk turbulence levels tended to be under predicted as compared to reality, possibly as a result of our coarse mesh within the grid itself. The circulation values are also predicted better for the split vane geometries as compared to the swirl geometries.

9 Acknowledgements

The authors would like to acknowledge the support of the Canadian Nuclear Safety Commission for funding this work. In particular the authors would like to acknowledge the input and discussions from Jacek Szymanski whose valuable insights helped improve this work at every stage.

10 References

[1] Chang S.K., Moon S.K., Baek W.P. and Choi Y.D., Phenomenological investigation on the turbulent flow structures in a rod bundle array with mixing vanes, Nuclear Engineering and Design, 238(2008), 600-609.

[2] Chang S.K., Moon S.K., Baek W.P. and Chun T.H., The experimental study on mixing characteristics in a square subchannel geometry with typical flow deflectors, Heat Transfer Engineering, 29(2008), 695-703.

[3] Holloway M.V., Fluid Dynamics and Heat Transfer of Turbulent Flow in Rod Bundle Subchannels, PhD Thesis, Clemson University, 2005.

[4] Holloway M.V., Conover T.A., McClusky H.L., Beasley D.E. and Conner M.E., The effect of support grid design on azimuthal variation in heat transfer coefficient for rod bundles, Journal of Heat Transfer, V. 127, pp. 598-605, 2005

[5] Holloway M.V., McClusky H.L., Beasley D.E. and Conner M.E., The effect of support grid features on local single-phase heat transfer measurements in rod bundle, Journal of Heat Transfer, V. 126, pp. 43-53, 2004

[6] McClusky H.L., Holloway M.V., Beasley D.E. and Conner M.E., Development of swirling flow in a rod bundle subchannel, Journal of Fluids Engineering, V. 125, pp. 747-755, 2002

[7] McClusky H.L., Holloway M.V., Conover T.A., Beasley D.E. Conner M.E. and Smith III L.D., Mapping of the lateral flow field in typical subchannels of a support grid with vanes, Journal of Fluids Engineering, V. 125, pp. 987-996, 2003.

[8] Conner M.E., Baglietto E.. and Elmahdi M.E., CFD methodology and validation for single-phase flow in PWR fuel assemblies, OECD/NEA & IAEA Workshop, Grenoble, France, 10-12 September 2008.

[9] Holloway M.V., Beasley D.E. and Conner M.E., Investigation of swirling flow in rod bundle subchannels using computational fluid dynamics, ICONE14-89068, Proceedings of ICONE14, Miami, Florida, USA, July 17-20, 2006

[10] In W.K., Numerical study of coolant mixing caused by the flow deflectors in a nuclear fuel bundle, Nuclear Technology, V. 134, pp. 187-195, 2001.

[11] Dominquez-Ontiveros E.E. and Hassan Y.A., Non-intrusive experiments investigation of flow behavior inside a 5x5 rod bundle with spacer grids using PIV and MIR, Nuclear Engineering and Design, 239(2009), 888-898.

[12] adapted from a presentation from B.L. Smith on OECD/NEA writing groups on the use of CFD for NRS issues, Technical meeting on application of CFD to NRS issues, IAEA HQ, Vienna, 14-16DEC, 2010.

[13] Lee J.R., Kim J. And Song C.-H., Synthesis of the OECD/NEA-KAERI rod bundle CFD benchmark exercise, Keynote lecture presented at CFD4NRS-4 conference, Daejeon, Korea, SEP2012.